



## Top-quark physics at colliders

Werner Bernreuther<sup>a</sup>, Peter Uwer<sup>b</sup><sup>a</sup>*Institut f. Theoretische Teilchenphysik u. Kosmologie, RWTH Aachen University, 52056 Aachen, Germany*<sup>b</sup>*Institut für Physik, Humboldt-Universität zu Berlin, 10099 Berlin, Germany*

---

### Abstract

Results are reviewed which were obtained within the project *Top-quark physics at colliders*. These include QCD and weak-interaction corrections to hadronic  $t\bar{t}$  production, determinations of the top-quark mass, predictions of the  $t\bar{t}$  charge asymmetry and  $t\bar{t}$  spin correlations, NLO QCD corrections to hadronic  $t\bar{t} + 1$ -jet production, and partial results for hadronic  $t$ -channel single-top production at NNLO QCD. In addition, some methodical developments made in this project are outlined, which are relevant for NLO and NNLO QCD calculations.

**Keywords:** Top quarks, QCD and weak corrections, NNLO antenna subtraction, NNLO integral reduction techniques

---

### 1. Introduction

When this project was started within this Collaborative Research Centre (SFB-TR-09) in January 2003, the top quark was still a rather unexplored particle as compared to lighter quarks and gauge bosons. The top quark was discovered at the Tevatron [1, 2] in 1995. The Tevatron collider Run 2 had just started in March 2001, and by the end of 2002, only of the order of about 1000 top-quark top-antiquark ( $t\bar{t}$ ) pairs had been produced at this collider. The ( $t\bar{t}$ ) cross section was measured, but with a rather large uncertainty of about 30% (cf., for instance, [3]). The combined result of the CDF and DØ determinations of the top-quark mass was  $m_t = 174.3 \pm 5.1$  GeV [3]. At this level of uncertainty, the question how this mass parameter is to be interpreted, i.e., is related to an appropriately defined Lagrangian mass parameter of the top quark, was not yet urgent. At that time, neither of the two Tevatron experiments had conclusive evidence for single top-quark production. Evidence for this production mode was reported only quite some time later by the DØ experiment [4]. On the theoretical side, results within the Standard Model (SM) included the computations at next-to-leading order (NLO) QCD of the hadronic production cross sections of top-quark pairs for unpolarized [5, 6, 7] and polarized [8] ( $t\bar{t}$ ), and

of single top quarks [9, 10, 11].

During the last twelve years tremendous progress has been made in the exploration of the properties and interactions of top quarks, both experimentally—especially since the Large Hadron Collider (LHC) started operating—and on the theoretical side. Significant theoretical contributions to this research topic were made within this Collaborative Research Centre and in particular within this project (C4). The main results on top-quark physics obtained in this project will be reviewed here.

The article is organized as follows. In Sect. 2 we review recent results obtained in project C4 related to the theoretical description of top-quark pair production. In particular, threshold corrections due to (would-be) bound-states and weak corrections are discussed. Furthermore, the first direct determination of the top-quark running mass from cross section data is described. In addition, results for less inclusive quantities, like the top-quark forward-backward charge asymmetry and spin correlations are presented. In Sect. 3 the NLO corrections to top-quark pair production in association with an additional jet are reviewed. In Sect. 4 we report on recent progress towards single top-quark production in next-to-next-to-leading order (NNLO) QCD.

Possible new physics contributions to top-quark decay  $t \rightarrow Wb$  are discussed in Sect. 5. Sect. 6 is devoted to methods and tools. We briefly outline the calculation of the so-called antenna functions for the production of a heavy quark-antiquark pair by an uncolored initial state at NNLO QCD and address the NNLO QCD calculations of the vector, axial-vector, scalar and pseudoscalar heavy-quark form factors. In addition we discuss an algorithm developed recently for the speed-up of the Laporta reduction algorithm. Furthermore, we discuss the automatic generation of the Catani-Seymour subtraction terms used in one-loop calculations.

## 2. Hadronic top-quark pair production

### 2.1. The $t\bar{t}$ cross section

In hadronic collisions top-quark pairs are dominantly produced via the strong interaction. In Born approximation the partonic channels  $q\bar{q} \rightarrow t\bar{t}$  and  $gg \rightarrow t\bar{t}$  contribute. The corresponding Feynman diagrams are shown in Fig.1. The NLO QCD corrections were cal-

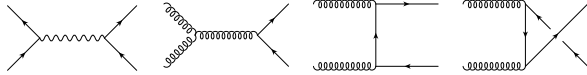


Figure 1: Born amplitudes contributing to top-quark pair production in hadronic collisions.

culated a long time ago [5, 6, 7]. Using the variation of the renormalization ( $\mu_r$ ) and factorization ( $\mu_f$ ) scales in the range  $m_t/2 < \mu_f, \mu_r < 2m_t$  for estimating the theoretical accuracy, an uncertainty at the level of  $\pm 12\%$  is found—clearly insufficient for the precision which is achieved at the LHC. To go beyond NLO predictions, an ansatz for the NNLO corrections based on soft gluon resummation was constructed in Ref. [12]. The idea is to use the general structure of soft gluon resummation as elaborated for example in Ref. [13] to predict the logarithms due to soft gluons in the fixed-order calculation. Extending the resummation formulae to next-to-next-to-leading logarithmic accuracy using an ansatz for the (at the time unknown) coefficient  $D_{Q\bar{Q}}^{(2)}$  appearing in the resummation formulae, all logarithmically enhanced terms were determined in Ref. [12]. Since NLO QCD corrections to top-quark pair production in association with an additional jet are small [14, 15] it has been argued in Ref. [12] that corrections with additional hard gluons are small and predictions based on soft gluon resummation should give reliable results (see also the discussion in Sect. 3). More precisely, using the velocity

of the top-quark

$$\beta = \sqrt{1 - 4m_t^2/\hat{s}}$$

where  $m_t$  denotes the top-quark mass and  $\hat{s}$  the partonic center of mass energy, the contributions proportional to

$$\alpha_s^3 \ln^4(\beta), \alpha_s^3 \ln^3(\beta), \alpha_s^3 \ln^2(\beta), \alpha_s^3 \ln(\beta)$$

are predicted in Ref. [12]. In addition all explicitly scale dependent terms together with the Coulomb corrections have been included into an approximate NNLO prediction. Very recently, full NNLO results have been presented [16, 17, 18, 19]. It is interesting to study how close the approximate results are with respect to the full results. In Ref. [12] (Table 12) the result

$$\sigma_{t\bar{t}}^{\text{NNLO approx.}} = 7.94_{+0.07}^{-0.28} \text{ pb} \quad (1)$$

is quoted for  $p\bar{p}$  collisions at the Tevatron collider at 1.96 TeV. The number  $-0.28 \text{ pb} (+0.07 \text{ pb})$  denotes the shift in the cross section when  $\mu = \mu_f = \mu_r = 2m_t$  ( $\mu = m_t/2$ ) is used instead of  $\mu = m_t$ . Using the same setup as in Ref. [12] ( $m_t = 171 \text{ GeV}$  and the CTEQ6.5 PDF set) the full NNLO QCD predictions [19, 20, 21] lead to

$$\sigma_{t\bar{t}}^{\text{NNLO}} = 7.99_{+0.30}^{-0.43} \text{ pb.} \quad (2)$$

While the theoretical uncertainty is underestimated in Ref. [12] the central value is in perfect agreement. The deviation is less than one per cent. For the LHC operating at 14 TeV the result quoted in Table 11 of Ref. [12] reads

$$\sigma_{t\bar{t}}^{\text{NNLO approx.}} = 918_{-39}^{-9} \text{ pb,} \quad (3)$$

while the full NNLO QCD result gives

$$\sigma_{t\bar{t}}^{\text{NNLO}} = 976_{+33}^{-53} \text{ pb.} \quad (4)$$

Since at the LHC the cross section is less threshold dominated one can expect that predictions based on soft gluon resummation are less powerful. Indeed we find that the approximate NNLO QCD predictions are 58 pb smaller than the full result. In fact only 43 % of the full NNLO QCD corrections are due to soft gluon effects while 57 % are due to non-logarithmic NNLO corrections.

Very close to the threshold, in addition to the logarithmic enhancement due to soft gluon emission, also Coulomb corrections become important. As it is well known from  $e^+e^-$  annihilation, these corrections can be resummed, using a non-relativistic Green function. Schematically, the hadronic cross section for the production of a  $t\bar{t}$  system in the state  $T = {}^{2s+1}S_J^{[1,8]}$  ( $s$  denotes the spin state and the indices 1 for singlet and 8

for octet denote the color state,  $L = 0$  close to threshold) reads [22]:

$$M_{t\bar{t}} \frac{d\sigma_{H_1 H_2 \rightarrow T}}{dM_{t\bar{t}}} = \sum_{i,j} \int_{s_{\text{had}}}^1 d\tau \left( \frac{d\mathcal{L}_{ij}}{d\tau}(\tau, \mu_f) \right) \times F_{ij \rightarrow T}(\hat{s}, M_{t\bar{t}}^2, \mu_f^2) \frac{1}{m_t} \text{Im} G^{[1,8]}(M_{t\bar{t}} + i\Gamma_t). \quad (5)$$

The partonic center of mass energy squared is again denoted by  $\hat{s}$ , while  $s_{\text{had}}$  is the hadronic center of mass energy.  $M_{t\bar{t}}$  is the invariant mass of the top-quark pair. (Note that beyond leading order (LO),  $M_{t\bar{t}} \neq \hat{s}$ .) The partonic luminosities for the collisions of two hadrons  $H_1, H_2$  are defined through

$$\frac{d\mathcal{L}_{ij}}{d\tau}(\tau, \mu_f) = \int dx_1 dx_2 f_{i/H_1}(x_1, \mu_f) f_{j/H_2}(x_2, \mu_f) \delta(\tau - x_1 x_2), \quad (6)$$

where  $f_{i/H}(x, \mu_f)$  denote the parton distribution functions evaluated at the factorization scale  $\mu_f$  ( $\tau = \hat{s}/s_{\text{had}}$ ). The functions  $F_{ij \rightarrow T}(\hat{s}, M_{t\bar{t}}^2, \mu_f^2)$  describe the hard scattering cross section for the production of a  $t\bar{t}$  system in the state  $T$  close to threshold. Compact expressions were presented in Refs. [23, 24]. In (5)  $G^{[1,8]}$  denotes the non-relativistic Green function, which resums the ‘‘bound-state’’ corrections. Analytic expressions can be found in Refs. [25, 26].  $\Gamma_t$  is the finite width of the top-quark. In Ref. [22] the predictions have been improved through the resummation of soft gluon effects to NNLL accuracy. Assuming that the resummation of soft gluon effects and threshold effects do not interfere, soft gluon resummation only replaces the cross sections  $F_{ij \rightarrow T}(s, M_{t\bar{t}}^2, \mu_f^2)$  by their resummed counterparts. To avoid double counting, the resummed results are matched to the fixed order result. Technically, the resummation is most conveniently performed in Mellin space following the methods illustrated for example in Ref. [13]. To avoid the evaluation of the inverse Mellin transformation, the convolution with the parton luminosities can also be done in Mellin space. In Fig. 2 the differential cross section is shown as function of the invariant mass of the  $t\bar{t}$  system. For the top-quark mass, a pole mass of 172.4 GeV has been used, leading to a nominal production threshold of 344.8 GeV. As one can see, binding effects due to the attractive potential in the color-singlet state lead to a resonance structure just below the threshold. In the color-octet channel the potential is repulsive preventing the formation of a (would-be) bound-state. Owing to the short life-time of the top quark, it is impossible to observe toponium states. However, the change of the cross section in the threshold region could in principle be observed. As it is well known

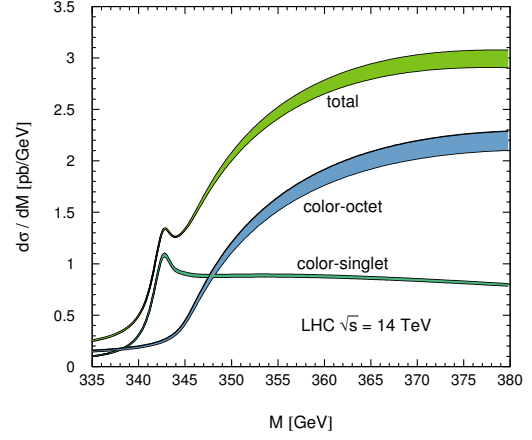


Figure 2: Bound state corrections to top-quark pair production [22]. Differential cross section in the threshold region as function of the invariant mass of the  $t\bar{t}$  system.

from linear collider studies, the peak position, being the remnant of a would-be bound state, is very sensitive to the value of the top-quark mass. Since the interesting region covers only 5 GeV in the invariant mass of the  $t\bar{t}$  system, the momentum resolution at the LHC is most likely insufficient to resolve this effect. Evidently, the region below the threshold will also give a contribution to the inclusive cross section. In Ref. [22] it has been estimated that binding effects could make an additional contribution of the order of 10 pb for LHC operating at 14 TeV, thus leading to a shift in the cross section predictions of about one per cent.

## 2.2. Weak interaction corrections

For predictions of the hadronic  $t\bar{t}$  cross section and differential distributions at a precision-level of a few percent, the electroweak corrections to hadronic  $t\bar{t}$  production must be taken into account. Sample diagrams are shown in Fig.3 for the  $q\bar{q}$  channel and in Fig.4 for the  $gg$  channel.

Weak interaction corrections to  $q\bar{q}, gg \rightarrow t\bar{t}$  were computed in Ref. [27]. The  $q\bar{q} \rightarrow t\bar{t}$  amplitude receives a tree-level contribution from  $s$ -channel  $Z$ -boson exchange. The nominally next-to-leading order weak corrections to the squared matrix element are the mixed QCD-weak corrections of order  $\alpha_s^2 \alpha$ . The mixed QCD-weak corrections to the squared  $gg \rightarrow t\bar{t}$  matrix element start at order  $\alpha_s^2 \alpha$ . In the analysis of Ref. [27] the box contributions to  $q\bar{q} \rightarrow t\bar{t}$ , which contain infrared divergences due to virtual soft gluons, and the quark triangle diagrams to  $gg \rightarrow Z^* \rightarrow t\bar{t}$  were left out. These contributions were taken into account in the computations

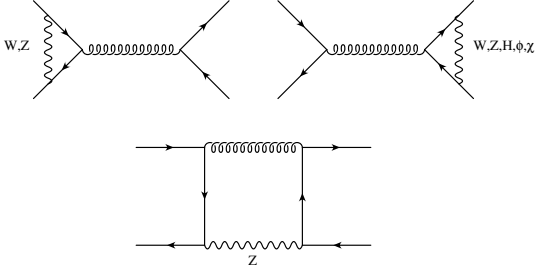
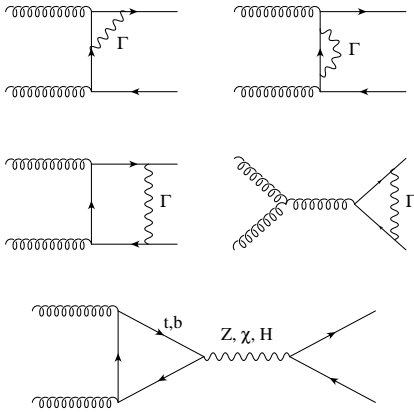


Figure 3: Sample diagrams for the weak corrections to top-quark pair production in quark–anti-quark annihilation.


 Figure 4: Sample diagrams for the weak corrections to top-quark pair production in gluon fusion. The label  $\Gamma$  denotes weak gauge bosons,  $H$ , and Goldstone bosons.

of the order  $\alpha_s^2\alpha$  QCD-weak corrections for  $q\bar{q} \rightarrow t\bar{t}(g)$  [28, 29] and for  $gg \rightarrow t\bar{t}$  [30, 31]. The results of these independent calculations were compared in detail and agree with each other. In Refs. [28, 30] also the  $t$ - and  $\bar{t}$ -spin dependent contributions to the respective squared matrix elements were calculated. These affect the polarization of  $t$ ,  $\bar{t}$  and the  $t\bar{t}$  spin correlations, see Sect. 2.5. Moreover, the weak-interaction corrections to  $qg$  and  $\bar{q}g$  initiated  $t\bar{t}$  production were determined in Ref. [32]. Recently, the mixed QCD-weak interaction corrections were re-evaluated for  $t\bar{t}$  production at the LHC for 8 and 14 TeV center-of-mass energy using up-to-date input for the Higgs boson mass, the top-quark mass, and parton distribution functions [33].

The order  $\alpha_s^2\alpha$  weak interaction corrections to the  $t\bar{t}$  cross section at the Tevatron are small; as compared with the NLO QCD cross section,  $\delta\sigma = \delta\sigma_W/\sigma_{\text{QCD}}^{\text{NLO}} = 0.5\%$ , where  $m_H = 125$  GeV was used. For the LHC (14 TeV)  $\delta\sigma = -1.27\%$  was obtained in Ref. [30] with CTEQ6.6M PDF and for  $\mu = m_t$ .

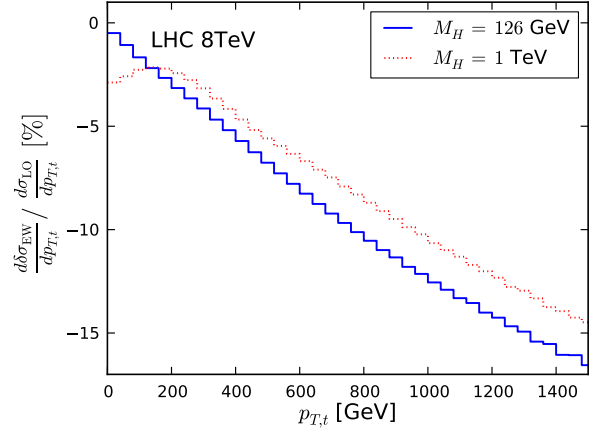


Figure 5: Weak corrections to transverse momentum distribution [33].

Although these weak-interaction corrections are nominally subdominant with respect to the QCD contributions, they become increasingly important at large  $t\bar{t}$  invariant mass and at large  $p_T^t$  due to the presence of weak Sudakov logarithms. This is illustrated in Fig. 5 where the weak-interaction corrections to the LO QCD  $p_T^t$ -distribution are shown.

A direct measurement of the top-quark Yukawa coupling provides important information to test the SM Higgs mechanism. It is well known that the Yukawa coupling leads to a positive contribution to the cross section in the threshold region due to the Sommerfeld enhancement. This is shown in Fig. 6 taken from Ref. [33] where the impact of an increased Yukawa coupling  $g_Y$  is plotted for a SM Higgs boson with a mass of 126 GeV. For comparison also the result for a Higgs boson with a mass of 1 TeV is given. In Ref. [33] the sensitivity to the top-quark Yukawa coupling has been investigated by studying the cross section in the threshold region:

$$\begin{aligned} \left. \frac{\delta\sigma_{\text{EW}}^{8\text{TeV}}}{\sigma_{\text{LO}}} \right|_{m_{t\bar{t}} < 2m_t + 50\text{GeV}} &= (-3.54 + 3.16g_Y^2)\%, \\ \left. \frac{\delta\sigma_{\text{EW}}^{8\text{TeV}}}{\sigma_{\text{LO}}} \right|_{m_{t\bar{t}} < 2m_t + 100\text{GeV}} &= (-3.06 + 2.06g_Y^2)\%, \\ \left. \frac{\delta\sigma_{\text{EW}}^{8\text{TeV}}}{\sigma_{\text{LO}}} \right|_{m_{t\bar{t}} < 2m_t + 150\text{GeV}} &= (-2.84 + 1.54g_Y^2)\%. \end{aligned}$$

(In the conventions used here the SM value is given by  $g_Y = 1$ .) A tiny contribution linear in the Yukawa coupling due to a  $b$ -quark loop has been neglected. For the lowest cut, the relative corrections change by about 9% if the SM Yukawa coupling is replaced by twice the SM value.

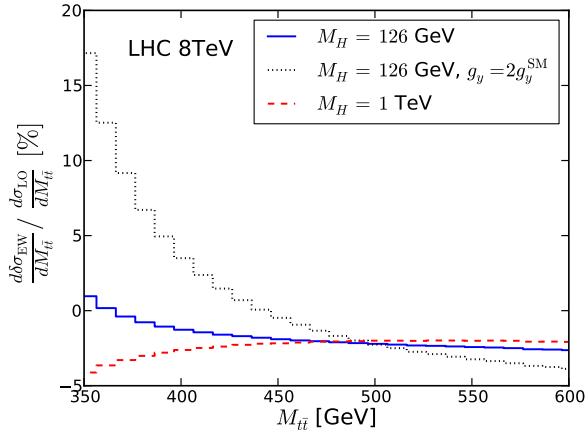


Figure 6: Relative weak corrections to the  $t\bar{t}$  invariant mass distribution in the framework of the SM assuming  $M_H = 126$  GeV (solid blue curve) and 1000 GeV (dashed red curve), and for the case of an enhanced Yukawa coupling  $g_Y = 2g_Y^{SM}$  with  $M_H = 126$  GeV (dotted black curve) [33].

### 2.3. Determination of the top-quark mass

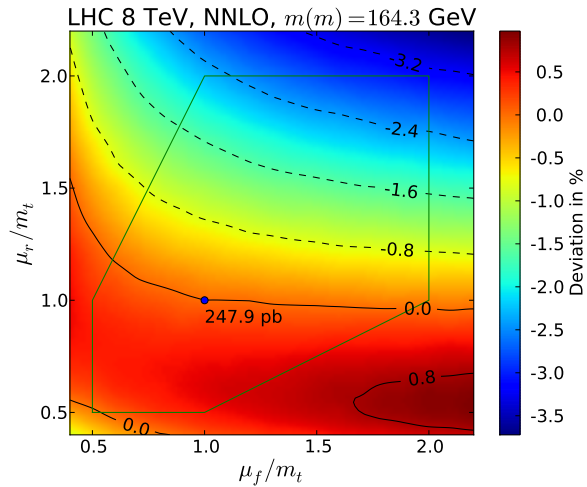


Figure 7: Scale (in)dependence of the inclusive  $t\bar{t}$  cross section at NNLO QCD using the  $\overline{\text{MS}}$  mass.

Including NNLO QCD corrections together with bound state effects and the weak corrections, the cross section predictions for inclusive top-quark pair production reach an accuracy at the level of a few per cent. These predictions can be compared with measurements in order to test the production mechanism. However, assuming the validity of the Standard Model, it is also possible to use the cross section measurements for the

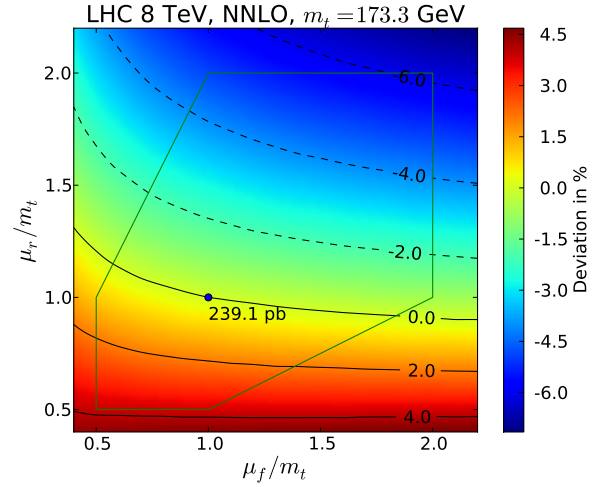


Figure 8: Same as Fig. 7 but for the pole mass.

determination of the top-quark mass, by fitting the theoretical predictions to the data. This is of particular interest since, contrary to measurements of the top-quark mass relying on the kinematical reconstruction of the top-quark decay products, the top mass entering the  $t\bar{t}$  cross section computed at higher order QCD is uniquely defined by the chosen renormalization scheme. Furthermore, different renormalization schemes for defining the top mass parameter can be employed. Using for example the running mass  $m(\mu)$  defined in the minimal subtraction ( $\overline{\text{MS}}$ ) scheme, an improved behavior of the perturbative expansion is observed. In Ref. [34] the inclusive cross section was expressed in terms of the running mass. In Fig. 7 the scale dependence of the cross section predictions using the  $\overline{\text{MS}}$  mass, calculated with the Hather program [21], is illustrated. For comparison, the scale dependence using the top-quark pole mass is shown in Fig. 8. As can be seen from Figs. 7, 8, the scale dependence is significantly reduced using the  $\overline{\text{MS}}$  mass instead of the pole mass. Using the pole mass, the cross section changes by about  $-6$  to  $+0.5$  percent, varying the scales between  $m_t/2$  and  $2m_t$ . For the  $\overline{\text{MS}}$  mass the variation is reduced to the range  $-3.2$  and  $0$  percent. The polygon in Fig. 7 shows the region of restricted scale variation used in NNLL predictions to define the scale uncertainty. The restricted range avoids extreme ratios of  $\mu_f/\mu_r$ . In difference to the NNLL results (not shown here) the improvement of the scale (in)dependence obtained using the  $\overline{\text{MS}}$  mass is independent on the precise definition of the restricted region.

In Ref. [34] the Tevatron cross section measurements were used to determine the top-quark mass. This is

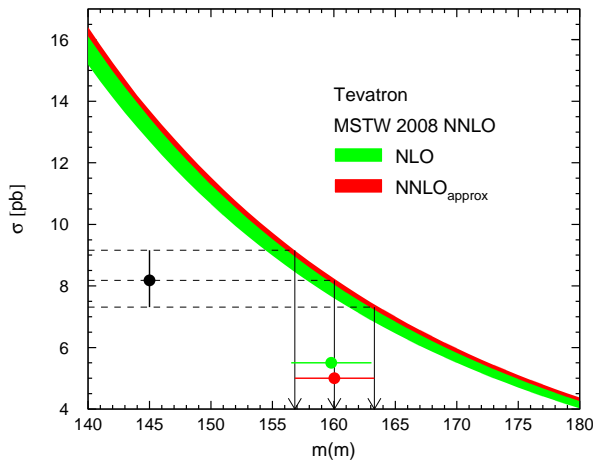


Figure 9: Determination of the running top-quark mass from cross section measurements [34]. The cross section as measured in Ref. [35] is projected onto the theoretical predictions.

illustrated in Fig. 9 taken from Ref. [34]. Projecting the measured cross section onto the NLO and NNLO (approx.) predictions, the running top-quark mass can be read off. Note that in this analysis, only the experimental uncertainties have been taken into account, since they are by far dominating. In particular, only the theoretical predictions for  $\mu = \mu_f = \mu_r = m(m)$  are compared to the data. (The results for  $\mu = 2m(m)$  and  $\mu = m(m)/2$  are both lower than the result for  $\mu = m(m)$ . The result for  $\mu = m(m)$  thus defines the upper boundary of the uncertainty band.) In Tab. 1 the extracted mass values are shown as determined in Ref. [34]. The

Table 1: The LO, NLO and approximate NNLO QCD results for the top-quark mass in the  $\overline{\text{MS}}$  scheme ( $m(m)$ ) and the pole mass scheme ( $m_t$ ) for the measured cross section of  $\sigma = 8.18\text{pb}$  at the Tevatron [35]. The uncertainties given in the Table reflect the quoted experimental uncertainties.

	$m(m)$ [GeV]	$m_t$ [GeV]
LO	$159.2^{+3.5}_{-3.4}$	$159.2^{+3.5}_{-3.4}$
NLO	$159.8^{+3.3}_{-3.3}$	$165.8^{+3.5}_{-3.5}$
NNLO	$160.0^{+3.3}_{-3.2}$	$168.2^{+3.6}_{-3.5}$

extraction has been performed using theoretical predictions at LO, NLO and NNLO (approx.) QCD. The results obtained for the running top-quark mass are very stable with respect to the order in perturbation theory. This is a direct consequence of the observation made in Ref. [34], that the convergence of the perturbative expansion is improved using the  $\overline{\text{MS}}$  mass. Furthermore, the results are compatible with the measurements based on the kinematic reconstruction. For comparison the outcome of the same procedure using instead the top-quark pole mass is also shown in Tab. 1. Large differences between the results obtained in different orders can be observed. The measurement of the top-quark mass as presented in Ref. [34] represents the first direct determination of the top-quark running mass. Since the cross section depends only weakly on the top-quark mass—a one per cent variation of the mass leads only to a five per cent variation of the cross section—it is very difficult, if not impossible, to reach an accuracy of better than 1 GeV. Nevertheless, the measurement provides an important cross check and has been repeated by the ATLAS and CMS experiments.

#### 2.4. The $t\bar{t}$ charge asymmetry

Charge asymmetries, or forward-backward asymmetries, were proposed and used first for  $e^-e^+$  production

of charged lepton pairs  $\ell^-\ell^+$  and of  $b\bar{b}$  pairs. They provide a test of the  $f\bar{f}$  production dynamics. In the following we consider the hadroproduction of  $t\bar{t}$  pairs. The  $t\bar{t}$  charge asymmetry is defined by

$$A_{\text{charge}} = \frac{N(y_t > 0) - N(y_{\bar{t}} > 0)}{N(y_t > 0) + N(y_{\bar{t}} > 0)}, \quad (7)$$

where  $y_t, y_{\bar{t}}$  denote the rapidities of  $t$  and  $\bar{t}$  in the laboratory frame. An asymmetry  $A_{\text{charge}} \neq 0$  is generated by the interference of terms in the scattering amplitude which are even and odd under interchange of  $t$  and  $\bar{t}$ , while the initial hadrons stay put.

$$d\sigma = d\sigma_S + d\sigma_A, \quad d\sigma_A(t, \bar{t}) = -d\sigma_A(\bar{t}, t).$$

The charge asymmetry in  $p\bar{p}, pp \rightarrow t\bar{t}X$  is primarily a NLO QCD effect, but electroweak corrections make a non-negligible contribution, too (see below).

For  $t\bar{t}$  production at the Tevatron, it is straightforward to show that, assuming CP invariance, the charge asymmetry is equal to the forward-backward asymmetry  $A_{\text{FB}}^t$ , i.e. the number of  $t$  quarks produced in the forward direction minus the number of  $t$  quarks produced in the backward direction divided by the total number of events. Most of the measurements of the Tevatron experiments CDF and D0 were made for the pair asymmetry

$$A^{\bar{t}t} = \frac{N(\Delta y > 0) - N(\Delta y < 0)}{N(\Delta y > 0) + N(\Delta y < 0)}, \quad (8)$$

where  $\Delta y = y_t - y_{\bar{t}}$  is the difference of the  $t$  and  $\bar{t}$  rapidities. For kinematical reasons  $A^{\bar{t}t}$  is larger than the laboratory-frame asymmetry (7).

The charge asymmetry/forward-backward asymmetry is generated in QCD to  $\mathcal{O}(\alpha_s^3)$  by the interference of terms in the scattering amplitudes of  $q\bar{q} \rightarrow t\bar{t}$ , and likewise of  $q\bar{q} \rightarrow t\bar{t}g$  which are even and odd under  $t \leftrightarrow \bar{t}$ . The reactions  $gq(\bar{q}) \rightarrow t\bar{t}q(\bar{q})$  contribute, too, but make only a very small contribution to the inclusive asymmetry at the Tevatron. Because of Bose symmetry  $gg \rightarrow t\bar{t}X$  does not contribute. The net effect for  $t\bar{t}$  production at the Tevatron is a difference in the rapidity distributions of  $t$  and  $\bar{t}$ : slightly more  $t$  ( $\bar{t}$ ) are produced in the forward direction  $y_t > 0$  (backward direction  $y_{\bar{t}} < 0$ ) than in the backward direction (forward direction).

The  $t\bar{t}$  charge asymmetry for the Tevatron was computed in QCD first in Ref. [36], including an estimate of the electroweak corrections. The mixed QCD-weak corrections were taken into account in Ref. [37]. In Ref. [38] it was shown that the mixed QCD-QED corrections are significant.

In recent years this observable has caused considerable excitement, because the first measurements of  $A_{\text{FB}}^t$

and  $A^{\bar{t}t}$  and their dependence on  $\Delta y$  and on the  $t\bar{t}$  invariant mass  $M_{\bar{t}t}$  showed deviations from the SM predictions up to  $\sim 3\sigma$ . For a recent review of the extensive literature on attempts to explain these apparent discrepancies by models for physics beyond the SM, see Ref. [39].

In Tab. 2 recent SM predictions for the Tevatron asymmetry  $A^{\bar{t}t}$  (inclusive and for  $M_{\bar{t}t} > 450$  GeV) are compiled. The result of Ref. [40] was obtained in QCD at NLO in  $\alpha_s$  including threshold resummation at NNLL accuracy, while the predictions of Refs. [38, 41, 42] were made, for different PDF sets, at fixed order NLO QCD including electroweak corrections. The electroweak corrections are significant, they amount to  $\sim 23\%$  of the QCD effect. The asymmetry  $A^{\bar{t}t}$  was also calculated differentially in bins of the modulus of the rapidity difference  $|\Delta y| = |y_t - y_{\bar{t}}|$ , cf. the references cited above. Very recently  $A^{\bar{t}t}$  was also computed at NNLO QCD in Ref. [43] with the result  $A^{\bar{t}t} = 0.095 \pm 0.007$  which includes electroweak corrections. Collider-independent forward-backward asymmetries, which apply to  $t\bar{t}$  production both at the Tevatron and the LHC, were analyzed in Ref. [44].

Table 2: SM predictions for the  $t\bar{t}$  charge asymmetry at the Tevatron.

	$A^{\bar{t}t}$ [%]	$A^{\bar{t}t}(M_{\bar{t}t} > 450 \text{ GeV})$ [%]
AFNPY [40]	$7.24^{+1.06}_{-0.72}$	$11.1^{+1.7}_{-0.9}$
HP [38]	$8.9^{+0.8}_{-0.6}$	$12.8^{+1.1}_{-0.9}$
KR [41]	$8.7 \pm 1.0$	$12.8 \pm 1.1$
BS [42]	$8.7 \pm 0.6$	$12.9 \pm 0.7$

Table 3: Recent experimental results on the  $t\bar{t}$  charge asymmetry at the Tevatron by the CDF [45] and D0 [46] experiments. The D0 result for  $A^{\bar{t}t}$  in bins of  $M_{\bar{t}t}$  agrees with the SM predictions compiled in Tab. 2.

	$A^{\bar{t}t}$ [%]	$A^{\bar{t}t}(M_{\bar{t}t} \geq 450 \text{ GeV})$ [%]
CDF [45]	$16.4 \pm 4.7$	$29.5 \pm 6.6$
D0 [46]	$10.6 \pm 3.0$	

The most recent measurements of the asymmetry  $A^{\bar{t}t}$  by the CDF [45] and D0 [46] experiments at the Tevatron are given in Tab. 3. The inclusive measurements agree quite well with the NLO SM predictions compiled in Tab. 2, while the CDF high mass asymmetry is still  $\sim 2.4\sigma$  above the SM predictions. However, the recent

$D0$  measurement [46] of  $A^{\bar{t}t}$  in bins of  $M_{\bar{t}t}$  (and in bins of  $|\Delta y|$ ) are consistent with the corresponding SM results.

### Top-quark charge asymmetry at the LHC

At the LHC, the initial  $pp$  state is in a parity eigenstate. Therefore, the integrated forward-backward laboratory-frame asymmetry vanishes:  $A_{\text{FB}}^t = A_{\text{FB}}^{\bar{t}} = 0$ . The parton distribution functions imply that in  $pp$  collisions, the reactions  $q\bar{q} \rightarrow t\bar{t}(g)$  ( $q = u, d$ ) are dominated by  $q$  with large  $x_q$  and  $\bar{q}$  with small  $x_{\bar{q}}$ . The QCD production of  $t\bar{t}$  then leads to  $t$  ( $\bar{t}$ ) quarks which are preferentially emitted in the direction of the incoming  $q$  ( $\bar{q}$ ). In the laboratory frame this means that in the forward and backward region there are more  $t$  than  $\bar{t}$ , while it is opposite in the central region. Using the difference of rapidity-moduli  $\Delta|y| = |y_t| - |y_{\bar{t}}|$ , a charge asymmetry  $A_C$  for  $t\bar{t}$  production at the LHC, which is non-zero within the SM, can be defined by

$$A_C = \frac{N(\Delta|y| > 0) - N(\Delta|y| < 0)}{N(\Delta|y| > 0) + N(\Delta|y| < 0)}. \quad (9)$$

The fixed-order SM predictions (NLO QCD and electroweak corrections) of Ref. [41] and Ref. [42] (which use different PDF sets) are given, for the LHC at 7 and 8 TeV, in Tab. 4. At the LHC (7 TeV) the electroweak corrections amount to  $\sim 15\%$ . The measurements of  $A_C$  by the CMS [47, 48] and ATLAS [49] experiments, collected in Tab. 5, are compatible with these SM results. The asymmetry  $A_C$  was also calculated differentially [42] in bins of  $|\Delta y|$  and  $M_{\bar{t}t}$ . These results also agree with the corresponding measurements by ATLAS and CMS.

Table 4: SM predictions for the  $\bar{t}t$  charge asymmetry at the LHC.

	$A_C(7 \text{ TeV})$ [%]	$A_C(8 \text{ TeV})$ [%]
KR [41]	1.15(6)	1.01(5)
BS [42]	1.23(5)	1.11(4)

Table 5: Recent experimental results on the  $\bar{t}t$  charge asymmetry at the LHC.

	$A_C(7 \text{ TeV})$ [%]	$A_C(8 \text{ TeV})$ [%]
CMS [47, 48]	$-1.0 \pm 1.9$	$0.5 \pm 0.9$
ATLAS [49]	$0.6 \pm 1.0$	

### Lepton asymmetries in $\ell + \text{jets}$ and $\ell\ell$ final states

The measurement of the top-quark charge asymmetries at the Tevatron and the LHC is, in fact, a very difficult experimental task because it requires to ‘clean’ the data from detector effects and then to unfold the data by sophisticated techniques from the level of final-state hadronic jets and leptons to the level of the intermediate  $t$  and  $\bar{t}$  quarks. On the other hand, the top-quark charge asymmetry induces also asymmetries of the daughter leptons from semileptonic top-quark decay. Although these asymmetries are expected to be smaller than the corresponding ones for top quarks, because the charged lepton does not strictly follow the direction of its top-quark parent, the leptonic asymmetries are expected to be less dependent on detector resolution and unfolding and should allow for a more direct comparison between theory and experiment.

Leptonic charge asymmetries were analyzed in Ref. [37, 42] for the Tevatron and LHC. For the Tevatron  $\bar{t}t$  production and decay to dileptonic and semileptonic final states were considered,

$$p\bar{p} \rightarrow \bar{t}t + X \rightarrow \ell^\pm + \text{jets}, \quad \ell^+ \ell'^- + \text{jets}. \quad (10)$$

For these two types of events the following single lepton and dilepton charge asymmetries can be defined:

$$A^\ell = \frac{N(q_\ell \eta_\ell > 0) - N(q_\ell \eta_\ell < 0)}{N(q_\ell \eta_\ell > 0) + N(q_\ell \eta_\ell < 0)}, \quad (11)$$

$$A^{\ell\ell} = \frac{N(\Delta\eta_\ell > 0) - N(\Delta\eta_\ell < 0)}{N(\Delta\eta_\ell > 0) + N(\Delta\eta_\ell < 0)}, \quad (12)$$

where  $\eta_\ell$  denotes the pseudo-rapidity of  $\ell^\pm$ ,  $\Delta\eta_\ell = \eta_{\ell^+} - \eta_{\ell^-}$ , and  $q_\ell$  is the lepton charge. For the LHC, dileptonic final states were investigated:

$$pp \rightarrow \bar{t}t + X \rightarrow \ell^+ \ell'^- + \text{jets}. \quad (13)$$

Here a dileptonic charge asymmetry can be defined in the following way:

$$A_{\text{LHC}}^{\ell\ell} = \frac{N(\Delta|\eta_\ell| > 0) - N(\Delta|\eta_\ell| < 0)}{N(\Delta|\eta_\ell| > 0) + N(\Delta|\eta_\ell| < 0)}. \quad (14)$$

where  $\Delta|\eta_\ell| = |\eta_{\ell^+}| - |\eta_{\ell^-}|$ .

These leptonic charge asymmetries were computed in Ref. [42] at NLO in the SM gauge couplings (NLO QCD in  $\bar{t}t$  production and decay including electroweak corrections). The results are given in Tab. 6 and 7 without acceptance cuts, because the experimental results, which are also collected in these tables, were provided in this way. All experimental results are compatible with the theoretical predictions.

In conclusion, apart from the tension of the CDF high-mass  $\bar{t}t$  asymmetry with SM predictions, the  $\bar{t}t$  and

Table 6: SM predictions [42] for the dilepton and single lepton charge asymmetries at the Tevatron and corresponding results of the D0 and CDF experiments. The experimental results are taken from the review of Ref. [50].

	$A^\ell$ [%]	$A^{\ell\ell}$ [%]
BS [42]	$3.8 \pm 0.3$	$4.8 \pm 0.4$
D0 (dilepton)	$4.4 \pm 3.9$	$12.3 \pm 5.7$
D0 ( $\ell+$ jets)	$4.7 \pm 2.6$	
CDF (dilepton)	$7.2 \pm 6.0$	$7.6 \pm 8.1$
CDF ( $\ell+$ jets)	$9.4 \pm 3.2$	

Table 7: SM predictions [42] for the dilepton charge asymmetry at the LHC and corresponding results of the CMS and ATLAS experiments. The experimental results are taken from the review of Ref. [51].

	$A_{\text{LHC}}^{\ell\ell}$ (7 TeV) [%]	$A_{\text{LHC}}^{\ell\ell}$ (8 TeV) [%]
BS [42]	$0.70 \pm 0.03$	$0.64 \pm 0.03$
CMS	$1.0 \pm 1.6$	
ATLAS	$2.3 \pm 1.4$	

the leptonic charge asymmetries measured at the Tevatron and at the LHC are compatible with the corresponding SM results.

### 2.5. Top-quark polarization and $t\bar{t}$ spin correlations

A well-known property of the top quark, which sets it apart from the other quarks, is that it decays before being able to form a hadronic bound-state. This offers the unique possibility to explore the interactions of a bare quark, in particular top spin effects, that is,  $t$  and  $\bar{t}$  polarization and  $t\bar{t}$  spin correlations.

In this section we consider the production of  $t\bar{t}$  pairs at the Tevatron and at the LHC. The degree of top polarization and the strength of the correlation of the  $t$  and  $\bar{t}$  spins depends on the  $t\bar{t}$  production dynamics and, for a certain production dynamics, on the choice of reference axes which can be interpreted as  $t$ - and  $\bar{t}$ -spin quantization axes, see below. These top-spin effects induce characteristic angular distributions and correlations among the final-state leptons and/or jets originating from top-quark and anti-top-quark decay, which can be measured.

First, we discuss  $t\bar{t}$  production and decay into dileptonic and lepton plus jets final states within the SM. It is well-known that the charged lepton from top-quark decay  $t \rightarrow q\ell\nu_\ell$ ,  $q = b(s, d)$  has the largest, i.e. max-

imal top-spin analyzing power (due to the  $V - A$  type interaction). Therefore the dileptonic decay channels are the most suitable ones for measuring  $t\bar{t}$  spin correlations, while  $\ell^\pm +$  jets final states can be used to exploring  $t$  and  $\bar{t}$  polarization. A traditional way of investigating top-spin effects in  $t\bar{t}$  production proceeds as follows. For definiteness we consider first the dileptonic decay channels. One defines two reference axes  $\hat{\mathbf{a}}$  and  $\hat{\mathbf{b}}$  (unit vectors), the ' $t$ - and  $\bar{t}$ -spin quantization axis', respectively. One determines the  $\ell^+$  and  $\ell'^-$  directions of flight in the  $t$  and  $\bar{t}$  rest frames, respectively, and measures the double distribution of the angles  $\theta_+ = \angle(\hat{\ell}_+, \hat{\mathbf{a}})$  and  $\theta_- = \angle(\hat{\ell}_-, \hat{\mathbf{b}})$  in the  $t, \bar{t}$  rest frames. If no acceptance cuts are applied, this double angular distribution has the form (cf. Refs. [8, 52])

$$\frac{1}{\sigma} \frac{d^2\sigma}{d\cos\theta_+ d\cos\theta_-} = \frac{1}{4} \left( 1 + B_1 \cos\theta_+ + B_2 \cos\theta_- - C \cos\theta_+ \cos\theta_- \right). \quad (15)$$

The coefficients  $B_1$  and  $B_2$  encode the degree of polarization of the  $t$  and  $\bar{t}$  samples with respect to the axes  $\hat{\mathbf{a}}$  and  $\hat{\mathbf{b}}$ , respectively, while  $C$  is a measure of the correlation of the  $t$  and  $\bar{t}$  spins. The polarization degrees can be obtained from the slopes of the one-dimensional distributions

$$\frac{1}{\sigma} \frac{d\sigma}{d\cos\theta_\pm} = \frac{1}{2} (1 + B_{1,2} \cos\theta_\pm) \quad (16)$$

which follow from Eq. 15. The  $t$  and  $\bar{t}$  polarization degrees are given by

$$P(\hat{\mathbf{a}}) = \langle 2\mathbf{S}_t \cdot \hat{\mathbf{a}} \rangle, \quad \bar{P}(\hat{\mathbf{b}}) = \langle 2\mathbf{S}_{\bar{t}} \cdot \hat{\mathbf{b}} \rangle, \quad (17)$$

where  $\mathbf{S}_t, \mathbf{S}_{\bar{t}}$  denotes the  $t$  and  $\bar{t}$  spin operator, respectively. The following relations hold:

$$B_1 = P(\hat{\mathbf{a}}) \kappa_\ell, \quad B_2 = -\bar{P}(\hat{\mathbf{b}}) \kappa_\ell, \quad (18)$$

where  $\kappa_\ell$  is the top-spin analyzing power of the charged lepton from top decay. (In the convention used here,  $\kappa_{\ell^+} = \kappa_{\ell^-} = \kappa_\ell$ .) At NLO QCD its value is  $\kappa_\ell = 0.999$ . The correlation of the  $t$  and  $\bar{t}$  spins is given by

$$\langle (\mathbf{S}_t \cdot \hat{\mathbf{a}})(\mathbf{S}_{\bar{t}} \cdot \hat{\mathbf{b}}) \rangle = \frac{\mathcal{A}}{4}, \quad (19)$$

where  $\mathcal{A}$  denotes the double spin asymmetry

$$\mathcal{A} = \frac{N(\uparrow\uparrow) + N(\downarrow\downarrow) - N(\uparrow\downarrow) - N(\downarrow\uparrow)}{N(\uparrow\uparrow) + N(\downarrow\downarrow) + N(\uparrow\downarrow) + N(\downarrow\uparrow)}. \quad (20)$$

The following relation holds between  $\mathcal{A}$  and the correlation coefficient  $C$  of Eq. 15:

$$C = \mathcal{A} \kappa_\ell^2. \quad (21)$$

Instead of measuring the two-dimensional distributions one may consider the distribution of the variables  $\cos \theta_+ \cos \theta_-$  for any choice of reference axes  $\hat{\mathbf{a}}, \hat{\mathbf{b}}$  [52]. One obtains that

$$C = -9 \langle \cos \theta_+ \cos \theta_- \rangle. \quad (22)$$

For the  $\ell+$  jets (or the all jets) decay channels, relations analogous to Eqs. 15–22 hold. In the case of non-leptonic top-decay  $t \rightarrow b$  jet + jets, the analyzing power of the jet which is used to analyze the top spin, enters these formulae. Experimentally useful choices for this purpose are the  $b$  jet or the least-energetic non- $b$  jet. Both have top-spin analyzing power significantly smaller than one [53].

For some choices of reference axes, including the helicity basis (see below), the contributions from  $q\bar{q} \rightarrow t\bar{t}$  and  $gg \rightarrow t\bar{t}$  to the correlation coefficient  $C$  enter with opposite sign. If eventually no sign of new physics contributions to hadronic  $t\bar{t}$  production will be found, one may use these spin correlations for a detailed exploration of the parton content of the proton [8].

Hadronic  $t\bar{t}$  production is dominated by QCD. Simple tree-level considerations reveal the following: Near threshold the  $t\bar{t}$  pair produced by  $q\bar{q}$  annihilation is in a  $^3S_1$  state, while it is in a  $^1S_0$  state for  $gg \rightarrow t\bar{t}$ . At high energies, i.e., for top-velocity  $\beta_t \rightarrow 1$ , helicity conservation of the SM gauge interactions implies that  $t_R\bar{t}_L, t_L\bar{t}_R$  events dominate over  $t_R\bar{t}_R, t_L\bar{t}_L$ . Here, the labels  $R, L$  refer to helicity. For  $t\bar{t}$  production at the Tevatron, which is dominated by  $q\bar{q} \rightarrow t\bar{t}$  one expects therefore a large SM induced  $t\bar{t}$  spin-correlation for the choice  $\hat{\mathbf{a}} = \hat{\mathbf{b}} = \hat{\mathbf{p}}$ , where  $\hat{\mathbf{p}}$  is the direction of the proton beam. A slightly larger SM effect is obtained if one chooses  $\hat{\mathbf{a}}$  and  $\hat{\mathbf{b}}$  such that the  $t\bar{t}$  spin-correlation is maximal for tree-level  $t\bar{t}$  production by  $q\bar{q}$  annihilation—the so-called off-diagonal basis [54]. At the LHC, where the  $gg \rightarrow t\bar{t}$  production mode is dominant and the top quarks have, on average, more relativistic speeds than at the Tevatron, the helicity basis  $\hat{\mathbf{a}} = \hat{\mathbf{k}}_t \equiv \hat{\mathbf{k}}, \hat{\mathbf{b}} = \hat{\mathbf{k}}_{\bar{t}} \equiv -\hat{\mathbf{k}}$  (in the  $t\bar{t}$  zero-momentum frame) is a good choice. A larger SM effect is obtained if  $\hat{\mathbf{a}}$  and  $\hat{\mathbf{b}}$  are chosen such that the  $t\bar{t}$  spin-correlation is maximal for tree-level  $gg \rightarrow t\bar{t}$  production—the so-called maximal basis [55]. For the dileptonic decay channels the opening angle between the lepton directions of flight, determined in the  $t$ , respectively in the  $\bar{t}$  rest frame,  $\varphi = \angle(\hat{\ell}_+, \hat{\ell}_-)$  is another useful observable for tracing  $t\bar{t}$  spin correlations [56]. In the absence of acceptance cuts its distribution is of the form

$$\frac{1}{\sigma} \frac{d\sigma}{d \cos \varphi} = \frac{1}{2} (1 - D \cos \varphi), \quad (23)$$

and

$$D = \frac{4}{3} \langle \mathbf{S}_t \cdot \mathbf{S}_{\bar{t}} \rangle \kappa_\ell^2. \quad (24)$$

This observable samples the diagonal terms of the  $t\bar{t}$  production density matrices.

The observables discussed above are designed such that the distributions Eq. 15, Eq. 23 are flat if the polarization of  $t, \bar{t}$  and the  $t\bar{t}$  spin correlations are zero. On the other hand, for the measurement of these distributions, the  $t$  and  $\bar{t}$  rest frames have to be determined which is a difficult experimental task. From the experimental point of view, a simpler observable is the difference of the  $\ell^\pm$  azimuthal angles measured in the laboratory frame,  $\Delta\phi = \phi_{\ell^+} - \phi_{\ell^-}$ . Although the distribution  $\sigma^{-1} d\sigma/d\Delta\phi$  is non-flat even if the  $t$  and  $\bar{t}$  were completely uncorrelated, its shape is sufficiently distinct from the shape resulting from  $t$  and  $\bar{t}$  being fully correlated, see Fig. 10. This allows for an experimental discrimination.

Let us first discuss the polarization of the  $t$  and  $\bar{t}$  samples in hadronic  $t\bar{t}$  events. Because QCD is parity invariant, the strong interactions cannot induce a non-zero longitudinal polarization, i.e., a polarization in the production plane. The parity-violating weak interaction contributions to  $t\bar{t}$  production induce a nonzero but very small polarization  $P, \bar{P}$ . This SM-induced weak interaction polarization was computed in Refs. [30, 32, 57] for  $t\bar{t}$  production at the Tevatron and the LHC. The top-quark polarization  $P(\hat{\mathbf{k}})$  in the helicity basis was measured by ATLAS [58] and CMS in  $\ell+$  jets events at the LHC [59] (7 TeV). The results are given in Tab. 8, together with the SM prediction. The SM-induced polarization  $P(\hat{\mathbf{k}})$  increases somewhat with increasing hadronic center-of-mass energy  $\sqrt{s_{\text{had}}}$ , but does not exceed 1% for  $\sqrt{s_{\text{had}}} = 14$  TeV. For fixed  $\sqrt{s_{\text{had}}}$ , the polarization  $P(\hat{\mathbf{k}})$  increases for samples with large  $M_{t\bar{t}}$  due to the presence of weak Sudakov logarithms, but on the other hand, the event rate decreases rapidly. CP invariance implies that  $P(\hat{\mathbf{k}}) = \bar{P}(-\hat{\mathbf{k}})$ . The observables  $P(\hat{\mathbf{k}})$  and  $P(\hat{\mathbf{p}})$  are useful for the search for parity-violating new physics contributions to  $t\bar{t}$  production. Such contributions were discussed, for instance, in the context of the apparent discrepancy between the  $t\bar{t}$  charge asymmetry measured at the Tevatron and the corresponding SM predictions. (For a review and references, see Ref. [39].)

The absorptive parts of the  $t\bar{t}$  production amplitudes induce a polarization of the  $t$  and  $\bar{t}$  samples normal to the production plane (transverse polarization). The QCD-induced transverse polarization of  $t$  and  $\bar{t}$  were computed in Ref. [60] from the absorptive parts of the NLO QCD  $q\bar{q}, gg \rightarrow t\bar{t}$  amplitudes. This QCD-induced polar-

ization is also small. At the LHC (8 TeV)  $P(\hat{\mathbf{n}}) = \bar{P}(\hat{\mathbf{n}}) = 0.35\%$  ( $\hat{\mathbf{n}} = (\hat{\mathbf{p}} \times \hat{\mathbf{k}})/|\hat{\mathbf{p}} \times \hat{\mathbf{k}}|$ ).

Table 8: SM prediction [30, 32, 57] and experimental results for the polarization of  $t$  quarks along the helicity axis in  $t\bar{t}$  events at the LHC (7 TeV).

LHC (7 TeV)	SM	ATLAS [58]	CMS [59]
$P(\hat{\mathbf{k}})$ [%]	0.3	$-3.5 \pm 1.4$	$3.7 \pm 2.1$

Contrary to top-quark polarization, the correlation of the  $t$  and  $\bar{t}$  spins is a large effect in the SM, because it is induced already at lowest order QCD. Spin correlation effects, i.e., the distributions Eq. 15 and Eq. 23 were computed at NLO QCD in Refs. [8, 52] and, including weak interaction corrections, in Refs. [42, 57]. Some of these results, namely the helicity correlation and the opening angle distribution for dileptonic  $t\bar{t}$  events at the LHC, 7 and 8 TeV, are given in Tab. 9. In Refs. [42, 57] also the distribution  $\sigma^{-1}d\sigma/d\Delta\phi$  mentioned above was computed at this level of perturbation theory. It is shown in Fig. 10 for dileptonic  $t\bar{t}$  events at the LHC, 7 TeV. For comparison, also the resulting distribution is shown when the  $t\bar{t}$  spin correlations are switched off.

Table 9: SM predictions [42, 57] for the correlation coefficient  $C$  of the double distribution (15) in the helicity basis and of the correlation coefficient  $D$  in the opening angle distribution (23), at NLO QCD including weak interaction corrections, for dileptonic  $t\bar{t}$  events at the LHC, 7 and 8 TeV. The results given in this table were obtained by Taylor-expansion of the normalized distributions to next-to-leading order in the gauge couplings.

	$C_{\text{hel}}$	$D$
LHC (7 TeV)	0.310(6)	-0.223(4)
LHC (8 TeV)	0.318(5)	-0.228(5)

On the experimental side, evidence for  $t\bar{t}$  spin correlations were first reported by the  $D0$  experiment at the Tevatron [61] (with large experimental uncertainties, but consistent with the SM prediction). Observation of  $t\bar{t}$  spin correlations in dileptonic events was made first by the ATLAS experiment [62] at the LHC, by the measurement of the  $\Delta\phi$  distribution and the distribution of  $\cos\theta_+ \cos\theta_-$  in the helicity basis (cf. Eq. 22) for dileptonic  $t\bar{t}$  events at 7 TeV. More recently, these measurements were also made by the CMS experiment [59] and repeated by ATLAS [63] with higher statistics for a set of variables including the correlation in the maximal basis. All of these experimental results at the LHC agree

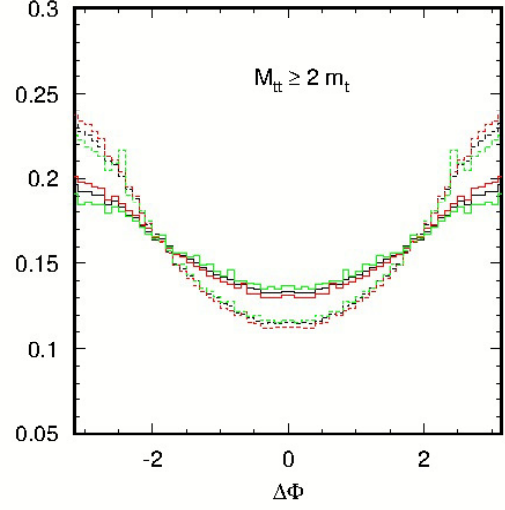


Figure 10: SM prediction for  $(\sigma^{-1}d\sigma/d\Delta\phi)_{SM}$  at NLO QCD including weak corrections of the normalized dilepton  $\Delta\phi$  distribution at the LHC (7 TeV). Dashed = uncorrelated, solid = correlated. The chosen scales are  $\mu = m_t$ (black),  $2m_t$  (red), and  $m_t/2$  (green). (Color code in online version only.) No cut on  $M_{t\bar{t}}$  was applied. From Ref. [57].

with the corresponding SM predictions. Measurements for  $t\bar{t}$  events recorded at 8 TeV are underway.

Nevertheless, the experimental precision achieved by ATLAS and CMS so far still does not preclude the possibility that there are new physics contributions to these  $t$ ,  $\bar{t}$  polarization and correlation observables of the order of several percent. There is a huge literature on new physics contributions to  $t\bar{t}$  production and decay, both within specific extensions of the SM and in the framework of effective field theory. Assuming that new physics effects in hadronic  $t\bar{t}$  production are induced by new heavy particle exchanges (characterized by a mass scale  $M$ ) one may construct a local effective Lagrangian  $\mathcal{L}_{eff}$  that respects the SM gauge symmetries and describes possible new physics interaction structures for energies smaller than  $M$ . Recent analyses include Refs. [64, 65, 66]. If one confines oneself to interactions of mass dimension 5 after spontaneous electroweak symmetry breaking then the new-physics part of  $\mathcal{L}_{eff}$  relevant for hadronic  $t\bar{t}$  production is given in terms of chromo dipole couplings of the top quark to the gluon(s):

$$\begin{aligned} \mathcal{L}_{eff} &= \mathcal{L}_{SM} \\ &- \frac{\tilde{\mu}_t}{2} \bar{t} \sigma^{\mu\nu} T^a t G_{\mu\nu}^a - \frac{\tilde{d}_t}{2} \bar{t} t \sigma^{\mu\nu} \gamma_5 T^a t G_{\mu\nu}^a, \end{aligned} \quad (25)$$

where  $\tilde{\mu}_t$  and  $\tilde{d}_t$  are the chromo-magnetic (CMDM) and chromo-electric (CEDM) dipole moment of the top quark, respectively,  $G_{\mu\nu}^a$  denotes the gluon field strength tensor, and  $T^a$  the generators of  $SU(3)$  color. In particular, a sizeable non-zero CEDM would signal a new type of CP-violating interaction beyond the Kobayashi-Maskawa CP phase.

It is customary to define dimensionless chromo moments  $\hat{\mu}_t, \hat{d}_t$  by

$$\tilde{\mu}_t = \frac{g_s}{m_t} \hat{\mu}_t, \quad \tilde{d}_t = \frac{g_s}{m_t} \hat{d}_t, \quad (26)$$

where  $m_t$  denotes the top-quark mass and  $g_s$  is the QCD coupling.

In Ref. [57] the top CMDM and CEDM contributions to a number of distributions related to top-spin effects were computed, and it was analyzed how these chromo moments distort the respective NLO SM predictions. The analysis of Ref. [57] is based on the following:

- i) Non-zero top CMDM and CEDM contribute also to the total  $t\bar{t}$  cross section. By comparison of the measured  $t\bar{t}$  cross section at the Tevatron and the LHC with respective predictions at NLO QCD one obtains correlated bounds on the dimensionless moments  $\hat{\mu}_t$  and  $\hat{d}_t$ . For a recent analysis, see Ref. [67]. These correlated bounds imply that the moduli of  $\hat{\mu}_t$  and  $\hat{d}_t$  must be significantly smaller than one, if non-zero at all. Therefore it is legitimate to take into account only contributions of  $\hat{\mu}_t$  and  $\hat{d}_t$  to the top-spin observables which are *linear* in these moments.
- ii) The anomalous interactions Eq. 25 are non-renormalizable. In a ultraviolet completion of the model the anomalous couplings  $\hat{\mu}_t$  and  $\hat{d}_t$  are limits of form factors which depend on (a) kinematic invariant(s) and they can have also absorptive parts if the 4-momentum transfer  $q^2$  in a gluon-top vertex is time-like, in particular if  $q^2 > 4m_t^2$ . Therefore, the following parameterization was used in Ref. [57]:

$$\hat{\mu}_t = \text{Re}\hat{\mu}_t + i\text{Im}\hat{\mu}_t, \quad \hat{d}_t = \text{Re}\hat{d}_t + i\text{Im}\hat{d}_t. \quad (27)$$

Imaginary parts were taken into account if the 4-momentum transfer  $q^2 > 4m_t^2$  in the respective gluon-top vertex. Notice that  $\hat{\mu}_t, \hat{d}_t$  parameterize by definition only new physics contributions to  $g_{tt}$  and  $gg_{tt}$  vertices. It is assumed that  $\hat{\mu}_t, \hat{d}_t$  are constants. As only normalized top-spin observables are considered, this assumption does not spoil perturbative unitarity.

- iii) No other top-decay mode than  $t \rightarrow Wb$  was observed so far. The  $t \rightarrow Wb$  decay amplitude

may also be affected by new physics contributions which can also be parameterized by anomalous couplings. From the experimental analysis of top-quark decay one knows that the moduli of these anomalous couplings must also be significantly smaller than one, if non-zero at all, see Sect. 5. Therefore, it is legitimate to take into account only anomalous contributions to  $t \rightarrow Wb$  which are *linear* in these moments. In Ref. [57] only distributions were analyzed where the charged lepton(s) act(s) as top spin analyzer(s). It has been shown [68, 69, 70] that, in this linear approximation, the charged-lepton angular distributions of polarized top-quark decay are not distorted by these couplings. That is, the top-spin analyzing power of the lepton retains its SM value  $\kappa_\ell = 0.985$ .

Items i) - iii) imply that the leptonic angular distributions for dileptonic and semileptonic  $t\bar{t}$  events receive only contributions from the complex top-quark chromo moments (Eq. 27). Moreover, distributions were used in Ref. [57] which transform in a definite way with respect to CP and naive  $T_N$  transformations. This implies that each of these distributions receives, in the linear approximation, a contribution from only one of the four moments (Eq. 27), but not from a combination of these moments.

For instance, the helicity and beam correlation, the opening angle distribution, and the  $\Delta\phi$  distribution receive a contribution from  $\text{Re}\hat{\mu}_t$  only. This result was recently used by the CMS experiment. From the comparison of the measured  $\Delta\phi$  distribution for dileptonic events at 7 TeV with the SM distribution, CMS derived the bound [71]

$$-0.043 < \text{Re}\hat{\mu}_t < 0.117 \quad @ \ 95\% \text{CL}.$$

A non-zero CEDM  $\text{Re}\hat{d}_t$  can be traced with CP-odd triple correlations. A suitable observable is

$$\mathcal{O}_{CP} = (\hat{\ell}_+ \times \hat{\ell}_-) \cdot \hat{\mathbf{k}}. \quad (28)$$

The SM contribution to its expectation values is negligible (recall that  $pp$  is not a CP eigenstate). For dileptonic  $t\bar{t}$  events at the LHC (8 TeV) one obtains [57]

$$\langle \mathcal{O}_{CP} \rangle = c \text{Re}\hat{d}_t, \quad c = -0.415(6). \quad (29)$$

The corresponding CP asymmetry is

$$\begin{aligned} A^{CP} &= \frac{N_{\ell\ell}(\mathcal{O}_{CP} > 0) - N_{\ell\ell}(\mathcal{O}_{CP} < 0)}{N_{\ell\ell}} \\ &= \frac{9\pi}{16} \langle \mathcal{O}_{CP} \rangle. \end{aligned} \quad (30)$$

This relation holds if no acceptance cuts are applied, but is valid also if cuts on  $M_{t\bar{t}}$  are made. This observable has not yet been measured. A systematic experimental search for anomalous top chromo moments by measuring spin observables has not yet been done.

### 3. Hadronic top-quark pair production in association with an additional jet

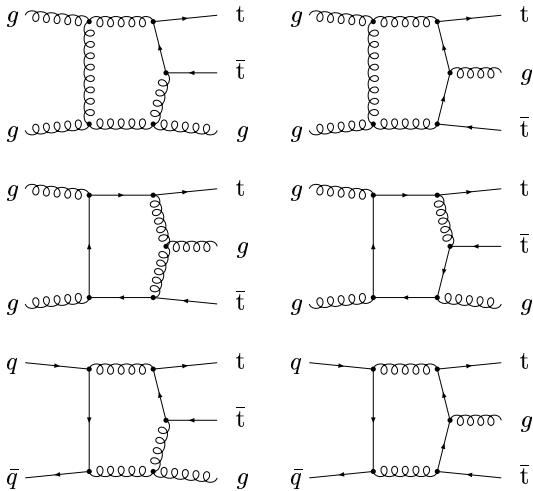


Figure 11: Pentagon topologies contributing to top-quark pair production in association with an additional jet.

A significant fraction of top-quark pair events produced in hadronic collisions is accompanied by an additional jet. For example, requiring a minimum transverse momentum of 50 GeV for the additional jet, about 30 per cent of the top-quark pair events are produced in association with a further jet. A precise theoretical understanding of the jet activity is thus mandatory for any top-quark analysis. Since LO QCD predictions suffer from a large scale dependence, reliable predictions can only be obtained by calculating the NLO corrections. Some sample diagrams contributing to  $t\bar{t} + 1$ -jet production at NLO QCD are shown in Fig. 11. In Refs. [14, 15] the NLO corrections have been calculated. For the virtual corrections two different algorithms for the reduction of one-loop tensor integrals to scalar one-loop integrals were used. In one calculation, the method developed in Ref. [72] is used to reduce the pentagon diagrams to scalar one-loop integrals. In the second calculation, the technique proposed in Ref. [73] has been applied. For the box and lower point topologies private implementations of the Passarino-Veltman [74] reduction procedure have been used. The virtual corrections were evaluated

using the spinor helicity formalism, allowing in principle to study also polarization dependent cross sections. For the real corrections Madgraph [75] generated code as well as a private implementation of the matrix elements has been used. The divergences in the real corrections were extracted using the Catani-Seymour subtraction formalism [76, 77]. In Ref. [14] the ‘inclusive’ jet cross section and the forward-backward charge asymmetry were studied. As expected, the inclusion of the NLO corrections leads to a significant reduction of the scale dependence of the cross section predictions. This is shown in Fig. 12 where results for the Tevatron and the LHC are given. (Note that the renormalization scale is set equal to the factorization scale.) In both cases, for the LHC and the Tevatron, a minimum transverse momentum of 20 GeV for the additional jet is required. The top-quark mass is renormalized using the pole mass scheme. The value  $m_t = 174$  GeV is used. In addition to the improved scale dependence, one can observe that around  $\mu = m_t$  the NLO corrections are very small and develop a plateau. This choice, i.e., setting the renormalization and factorization scale equal to the top-quark mass, thus provides a good convergence of the perturbative expansion. In Ref. [14] also the forward-backward charge asymmetry is calculated. While in inclusive top-quark pair production the asymmetry appears first at the one-loop order, in  $t\bar{t} + 1$ -jet production the asymmetry is already present in Born approximation. The NLO calculation thus allows to calculate also the higher order corrections for the charge asymmetry. The results obtained in Ref. [14] are shown in Fig. 13. As discussed in Sect.

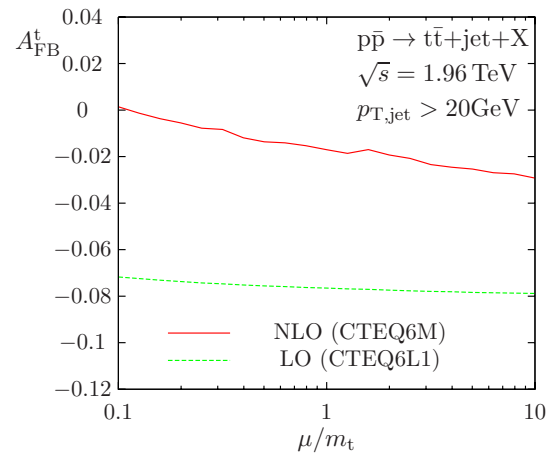


Figure 13: Next-to-leading order QCD corrections for the forward-backward charge asymmetry in  $p\bar{p} \rightarrow t\bar{t} + 1\text{-jet} + X$ . [14]

2.4 the charge asymmetry is defined as a cross section ratio. As a consequence, the leading power in  $\alpha_s$  can-

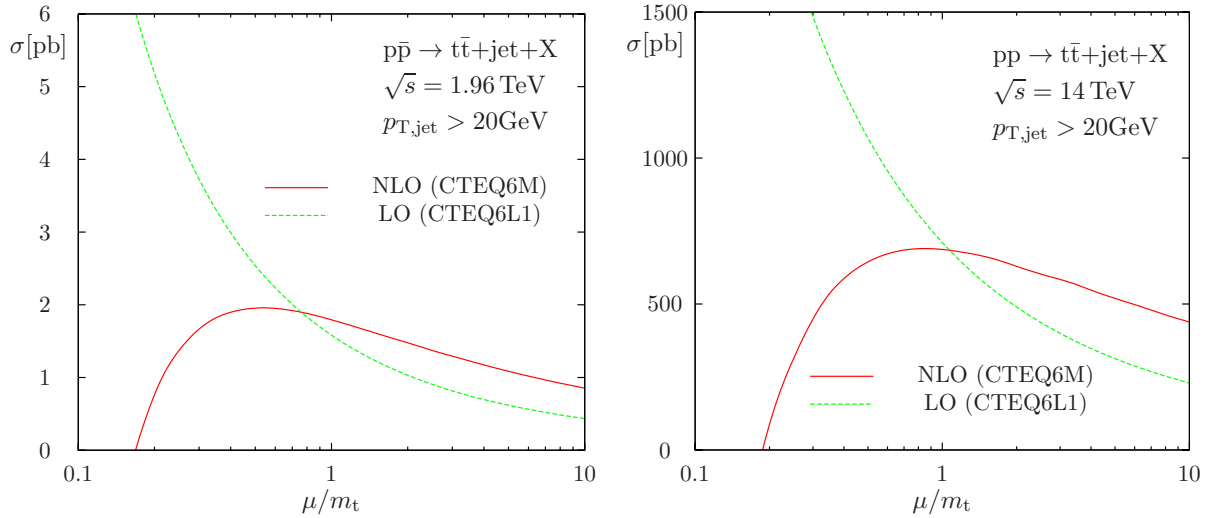


Figure 12: Scale dependence of the LO and NLO QCD cross section for  $t\bar{t} + 1$ -jet production. The top-quark mass is renormalized in the on-shell scheme.

cells. Furthermore, also the factorization scale dependence cancels to some extent between the numerator and the denominator. This explains the small scale dependence of the LO result shown in Fig. 13. Evidently, the scale variation does not provide a sensible estimate of the uncalculated higher order corrections. Indeed, Fig. 13 shows a very large shift of the predictions, when including the NLO corrections. While to Born approximation the asymmetry is of the order of  $-7\%$  to  $-8\%$ , at NLO QCD the prediction is reduced to the range  $0\%$  to  $-3\%$  depending on the chosen scale. It has been speculated that something similar could also happen in case of the inclusive  $t\bar{t}$  asymmetry, where until recently the predictions have been only leading-order in QCD. In Ref. [78] it has been argued that in  $t\bar{t} + 1$ -jet production the large corrections to the charge asymmetry are due to two different effects which appear at different orders in the perturbative expansion. Due to the recoil, hard gluon emission leads to a forward-backward charge asymmetry. This effect is present already in leading-order in the  $t\bar{t} + 1$ -jet asymmetry. Beyond leading-order, also soft gluon emission can contribute to the charge asymmetry. In  $t\bar{t} + 1$ -jet production this effect requires at least NLO accuracy and could be responsible for the large corrections. In contrast, in case of the inclusive asymmetry, both effects are present already in the leading order prediction. As a consequence no large corrections are expected [78].

In Ref. [15] the NLO corrections were extended to differential distributions. In particular, the dependence

Table 11: Cross section  $\sigma_{t\bar{t}+1\text{jet}}$  at the LHC (14 TeV) for different values of  $p_{T,\text{cut}}^{\text{jet}}$  for  $\mu = \mu_{\text{fact}} = \mu_{\text{ren}} = m_t$  [15]. The numbers in superscripts and subscripts are the shifts towards  $\mu = m_t/2$  and  $\mu = 2m_t$ , respectively.

$p_{T,\text{cut}}^{\text{jet}}$ [GeV]	$\sigma_{t\bar{t}+1\text{jet}}$ [pb]	
	LO	NLO
20	710.8(8) <sup>+358</sup> <sub>-221</sub>	692(3)3 <sup>-40</sup> <sub>-62</sub>
50	326.6(4) <sup>+168</sup> <sub>-103</sub>	376.2(6) <sup>+17</sup> <sub>-48</sub>
100	146.7(2) <sup>+77</sup> <sub>-47</sub>	175.0(2) <sup>+10</sup> <sub>-24</sub>
200	46.67(6) <sup>+26</sup> <sub>-15</sub>	52.81(8) <sup>+0.8</sup> <sub>-6.7</sub>

of the results on the transverse moment cut applied to the additional jet, was investigated.

Tab. 10 taken from Ref. [15] shows the results for  $p\bar{p}$  collisions at the Tevatron collider. In this case, positive corrections of about 13% are observed for the inclusive jet cross section, independent of the applied  $p_{T,\text{cut}}$ . Since the jet cross section diverges logarithmically for  $p_{T,\text{cut}} \rightarrow 0$ , the results increase for decreasing  $p_{T,\text{cut}}$ . In contrast, the asymmetry becomes increasingly negative with increasing  $p_{T,\text{cut}}$ . This is not surprising, since harder jets lead to an increased recoil of the top quarks. In addition the QCD corrections also increase with increasing  $p_{T,\text{cut}}$ .

In Tab. 11 the cut dependence is studied for the LHC (14 TeV). The NLO corrections are typically of the order of 15% and are only mildly dependent on the cut. As an example of a differential contribution calculated

Table 10: Cross section  $\sigma_{\bar{t}t\text{jet}}$  and forward–backward charge asymmetry  $A_{\text{FB}}^t$  at the Tevatron for different values of  $p_{T,\text{cut}}^{\text{jet}}$  for  $\mu = \mu_{\text{fact}} = \mu_{\text{ren}} = m_t$  [15]. The numbers in superscripts and subscripts are the shifts towards  $\mu = m_t/2$  and  $\mu = 2m_t$ , respectively. The uncertainty due to the numerical integration is given in parentheses.

$p_{T,\text{cut}}^{\text{jet}}$ [GeV]	$\sigma_{\bar{t}t\text{jet}}$ [pb]		$A_{\text{FB}}^t$ [%]	
	LO	NLO	LO	NLO
20	1.583(2) <sup>+0.96</sup> <sub>-0.55</sub>	1.791(1) <sup>+0.16</sup> <sub>-0.31</sub>	-7.69(4) <sup>+0.10</sup> <sub>-0.085</sub>	-1.77(5) <sup>+0.58</sup> <sub>-0.30</sub>
30	0.984(1) <sup>+0.60</sup> <sub>-0.34</sub>	1.1194(8) <sup>+0.11</sup> <sub>-0.20</sub>	-8.29(5) <sup>+0.12</sup> <sub>-0.085</sub>	-2.27(4) <sup>+0.31</sup> <sub>-0.51</sub>
40	0.6632(8) <sup>+0.41</sup> <sub>-0.23</sub>	0.7504(5) <sup>+0.072</sup> <sub>-0.14</sub>	-8.72(5) <sup>+0.13</sup> <sub>-0.10</sub>	-2.73(4) <sup>+0.35</sup> <sub>-0.49</sub>
50	0.4670(6) <sup>+0.29</sup> <sub>-0.17</sub>	0.5244(4) <sup>+0.049</sup> <sub>-0.096</sub>	-8.96(5) <sup>+0.14</sup> <sub>-0.11</sub>	-3.05(4) <sup>+0.49</sup> <sub>-0.39</sub>

in Ref. [15] we show in Fig. 14 the pseudo rapidity distribution of the top-quark in  $\bar{t}t + 1$ -jet events at the Tevatron. The distribution is asymmetric already at LO

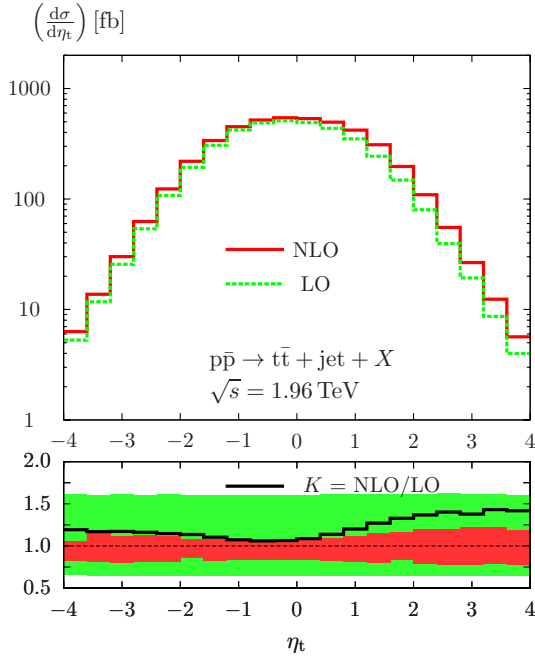


Figure 14: Pseudo-rapidity distribution of the top quark in  $\bar{t}t + 1$ -jet events at the Tevatron [15].

QCD, leading to the forward-backward charge asymmetry discussed before. In addition, it can be seen that the NLO corrections strongly depend on the rapidity, such that the leading-order asymmetry is almost washed out. Furthermore, the scale uncertainty is significantly reduced in the entire rapidity range. In addition to the rapidity distributions, the transverse momentum distribution of the top quark, the  $\bar{t}t$  system, and the additional jet has been investigated in Ref. [15] for the Tevatron and the LHC. While the first two distributions show a

moderate K-factor with only minor variations over the considered range, large corrections are observed at large  $p_T$  in case of the transverse momentum distribution of the additional jet. At high scale, the large transverse momentum of the jet introduces an additional energy scale different from the top-quark mass. In this situation the top-quark mass no longer corresponds to the typical energy scale of the problem. Using a phase-space dependent renormalization scale may thus lead to an improved behavior of the perturbation theory.

The findings of Refs. [14, 15] have been confirmed in Ref. [78, 79] where also the top-quark decay has been included. In Refs. [80, 81] the fixed-order predictions for  $\bar{t}t + 1$ -jet production are combined with the parton shower. Furthermore, the top-quark decay is included. The full spin information is taken into account in the top-quark decay. In Ref. [81] the impact of the parton-shower on various differential distributions is studied in detail. In particular, the forward-backward asymmetry is investigated. While the differences due to a different modeling (HERWIG/Pythia) of the parton shower are moderate, it turns out that the inclusion of the parton shower changes significantly the fixed order predictions. This is in agreement with the discussion presented before.

In Ref. [82] it has been argued that  $\bar{t}t + 1$ -jet events may be used to measure the top-quark mass. Since the gluon emission from a massive quark depends on the mass of the emitting quark, the additional jet may increase the sensitivity to the top-quark mass compared to the  $\bar{t}t$  inclusive cross section. For the ‘inclusive’ jet cross section, as shown for example in Tabs. 10, 11, it turns out that the sensitivity to the top-quark mass is however very similar to the respective sensitivity of the inclusive  $\bar{t}t$  cross section. To enhance the mass effect, it is thus important to focus on phase-space regions were

larger effects can be expected. In Ref. [82] the quantity

$$\mathcal{R}(m_t, \rho_s) = \frac{1}{\sigma_{\bar{t}\bar{t}+1\text{-jet}}} \frac{d\sigma_{\bar{t}\bar{t}+1\text{-jet}}}{d\rho_s}(m_t, \rho_s), \quad (31)$$

where  $\rho_s$  is defined as

$$\rho_s = \frac{2m_0}{\sqrt{s_{\bar{t}\bar{t}j}}} \quad (32)$$

is proposed. Here,  $m_0$  is an arbitrary mass scale of the order of the top-quark mass and  $s_{\bar{t}\bar{t}j}$  denotes the invariant mass of the  $\bar{t}\bar{t} + 1\text{-jet}$  final state (In Ref. [82]  $m_0 = 170$  GeV is used). For  $\rho_s \approx 0.8$  the observable  $\mathcal{R}$  becomes very sensitive to the top-quark mass. In this region a one percent variation of the mass leads roughly to a 20 percent variation of  $\mathcal{R}$ . A measurement of the distribution  $\mathcal{R}$  can thus be used to determine the top-quark mass. Since the mass is obtained through a fit of the theoretical predictions to the measured distribution, the mass is extracted in a well defined renormalization scheme—similar to the extraction from the inclusive  $\bar{t}\bar{t}$  cross section as discussed in Sect. 2.3. Very recently a first measurement of the top-quark mass using the  $\mathcal{R}$  observable has been presented by the ATLAS collaboration using the 7 TeV data [83]. The result

$$m_t = 173.7 \pm 1.5(\text{stat.}) \pm 1.4(\text{syst.})_{-0.5}^{+1.0}(\text{theo.}) \text{ GeV}$$

is in very good agreement with the measurements based on the kinematic reconstruction. Using a larger data set the statistical and to some extent also the systematic uncertainties will be reduced in the future—making the approach competitive with established methods.

#### 4. Hadronic production of single top quarks

While top quarks are dominantly produced in pairs in hadronic collisions, the flavor changing charged currents of the weak interaction allow also the single production of top quarks or anti-quarks. Single top-quark production is interesting, since it offers a sensitive probe to the weak interactions of the top quark. In particular, the  $V - A$  structure, as predicted in the SM, can be tested. In addition, single top-quark production provides a unique source of polarized top quarks. Furthermore, the process is sensitive to the last row of the CKM matrix, in particular to the matrix element  $V_{tb}$ . A precise measurement of single top-quark production can also be used to constrain the bottom PDF.

Feynman diagrams contributing to single top-quark production in leading-order are shown in Fig. 15. Depending on whether the momentum of the  $W$ -boson is space-like, time-like, or on-shell the production

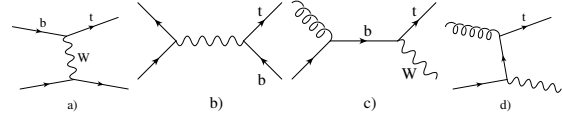


Figure 15: Feynman diagrams contributing to single top-quark production in leading order.

mechanism is called  $t$ -channel (Fig. 15 a),  $s$ -channel (Fig. 15 b), or  $Wt$  production (Fig. 15 c,d). The NLO QCD corrections for the different channels were calculated in Refs. [9, 10, 11, 84, 85, 86, 87, 88, 89]. An overview of the NLO predictions using recent input for the top-quark mass and the parton distribution functions is given in Tab. 12. For the  $t$ -channel, the most important channel both at the Tevatron and the LHC, the radiative corrections are very small. For the setup used in Tab. 12 the NLO contribution is of the order of a few percent. One may speculate, whether the corrections in the  $t$ -channel are accidentally small, because they are the result of a significant cancellation of individual contributions. Furthermore, owing to the simple color structure of the Born amplitude, only vertex corrections contribute to the NLO corrections. The box contributions vanish, when interfered with the Born amplitude. It is worth noting that at NLO QCD no color exchange is possible between the two quark lines. At NNLO QCD color exchange is no longer forbidden and may affect differential distributions.

Partial NNLO QCD results for the  $t$ -channel were calculated recently in Ref. [91]. Indeed, the corrections are about  $-50\%$  of the NLO corrections and larger than one would naively expect. (From a phenomenological perspective they are however very small and almost negligible given the currently achieved experimental uncertainty.) In Ref. [91] only the vertex corrections together with the corresponding real corrections are considered. In Ref. [92] the full set of two-loop  $t$ -channel corrections is studied as a step towards the complete result. The two-loop amplitude  $\mathcal{A}^{(2)}$  for  $u(k_u) + b(k_b) \rightarrow t(k_t) + d(k_d)$  defined through

$$\mathcal{A} = g_W^2 V_{tb} V_{ud}^* \left( \mathcal{A}^{(0)} + \frac{\alpha_s}{4\pi} \mathcal{A}^{(1)} + \left( \frac{\alpha_s}{4\pi} \right)^2 \mathcal{A}^{(2)} + \dots \right), \quad (33)$$

where  $g_W$  denotes the weak coupling, is further decomposed in Ref. [92] according to the color structure

$$\mathcal{A}^{(2)} = \delta_{tb} \delta_{du} A_1^{(2)} + \left( \delta_{tu} \delta_{db} - \frac{1}{N} \delta_{tb} \delta_{du} \right) A_2^{(2)}. \quad (34)$$

Table 12: Cross sections for single top-quark production in pb, for  $m_t = 173.3$  GeV,  $\mu = \mu_R = \mu_f = m_t$  and the MSTW2008lo/nlo PDF set, obtained using the Hathor program [21, 90]. The numbers in sub- and superscripts denote the uncertainty due to scale variation and PDF uncertainties. The scale uncertainty is estimated by varying the scale  $\mu$  from  $m_t/2$  to  $2m_t$ .

	LHC 13 TeV				Tevatron	
	$\sigma_t^{\text{LO}}$	$\sigma_{\bar{t}}^{\text{LO}}$	$\sigma_t^{\text{NLO}}$	$\sigma_{\bar{t}}^{\text{NLO}}$	$\sigma_{t,\bar{t}}^{\text{LO}}$	$\sigma_{t,\bar{t}}^{\text{NLO}}$
$t$	135	79.8	$137^{+4.0}_{-2.3}^{+1.0}_{-0.9}$	$82.1^{+2.5}_{-1.3}^{+0.6}_{-0.8}$	1.03	$0.998^{+0.025}_{-0.022}^{+0.029}_{-0.032}$
$s$	4.27	2.63	$6.25^{+0.06}_{+0.09}^{+0.12}_{-0.09}$	$3.97^{+0.04}_{+0.05}^{+0.08}_{-0.07}$	0.28	$0.442^{+0.023}_{+0.025}^{+0.015}_{-0.011}$
$tW$	29.1	29.1	$29.3^{+1.0}_{-1.3}^{+0.7}_{-0.8}$	$29.2^{+1.0}_{-1.3}^{+0.7}_{-0.8}$	0.069	$0.070^{+0.002}_{-0.001}^{+0.008}_{-0.009}$

Here,  $t, b, d, u$  are the color indices of the quarks,  $N$  is the number of colors ( $N = 3$  for QCD). Since the color structure of the Born amplitude is simply  $\delta_{tb}\delta_{du}$ , the second structure again vanishes when interfered with the Born amplitude. It is possible to decompose  $A_1^{(2)}$  further, into leading- and sub-leading color contributions:

$$A_1^{(2)} = (N^2 - 1) \left( A_{1,LC}^{(2)} + \frac{1}{N} T_r(B_h + n_l B_l) + \frac{1}{N^2} A_{1,SC}^{(2)} \right). \quad (35)$$

The contributions  $B_h$  and  $B_l$  are due to self-energy insertions in the one-loop topologies.  $B_h$  is due to a top-quark loop while  $B_l$  results from a massless quark loop, and  $n_l$  counts the number of massless quark flavors. In case of  $A_{1,LC}^{(2)}$ ,  $B_h$  and  $B_l$  only vertex corrections contribute. Sample diagrams are shown in Fig. 16. Two-loop topologies contributing to  $A_{1,SC}^{(2)}$  are shown

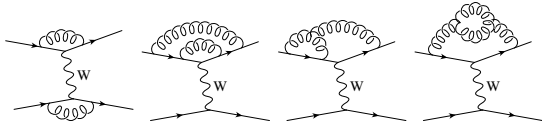


Figure 16: Sample topologies contributing to  $A_{1,LC}^{(2)}$ .

in Fig. 17. In Ref. [92] the amplitude is further de-

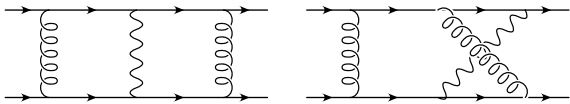


Figure 17: Sample diagrams contributing to  $A_{1,SC}^{(2)}$ .

composed into 11 different spin structures using a naive anti-commuting  $\gamma_5$ . Working with an anti-commuting

$\gamma_5$  is legitimate, since no anomaly is encountered in the present calculation and this prescription automatically preserves the Ward identities. The decomposition of  $A_1^{(2)}$  reads

$$A_1^{(2)} = \sum_{i=1} f_i \times \mathcal{S}_i \quad (36)$$

with

$$\begin{aligned} \mathcal{S}_1 &= \bar{u}(k_t) \gamma_7 u(k_b) \times \bar{u}(k_d) \gamma_6 \not{k}_t u(k_u), \\ \mathcal{S}_2 &= \bar{u}(k_t) \gamma_6 \not{k}_u u(k_b) \times \bar{u}(k_d) \gamma_6 \not{k}_t u(k_u), \\ \mathcal{S}_3 &= \bar{u}(k_t) \gamma_6 \gamma_{\mu_1} u(k_b) \times \bar{u}(k_d) \gamma_6 \gamma_{\mu_1} u(k_u), \\ &\vdots \end{aligned} \quad (37)$$

where  $u$  denotes a Dirac spinor and  $\gamma_6 = 1 + \gamma_5$ ,  $\gamma_7 = 1 - \gamma_5$ . To achieve the decomposition shown in Eq. 36 the two-loop tensor integrals have to be reduced at least partially, to get rid of the loop momenta appearing in the numerator. For the vertex corrections, two different techniques have been applied. One approach is to follow the method outlined in Refs. [93, 94] to reduce the tensor integrals to scalar integrals with raised powers of the propagators in higher dimensions of space-time. In a second step these integrals are then reduced to a small set of independent master integrals using the integration-by-parts (IBP) identities [95, 96]. In the second approach projectors are used to determine the scalar functions  $f_i$ . Calculating the trace after having multiplied with suitable projectors leads to scalar products of the loop-momenta with external momenta. These integrals can again be reduced using IBP relations. Technically, the reduction to the master integrals is done using the Laporta algorithm [97]. As main working horse, the publicly available implementation Reduze1/Reduze2 [98, 99] has been used in Ref. [92]. In addition, cross checks were made using a private version of the program Crusher [100]. To

check the setup and as additional cross check the vector and axial-vector form factor have been reproduced. For  $A_{1,LC}^{(2)}$ ,  $B_l$  and  $B_h$  and the vertex part of  $A_{1,SC}^{(2)}$  analytic results in terms of the known master integrals [101, 102, 103, 104, 105, 106, 107] are presented in Ref. [92]. As far as the double box topologies are concerned, only the projection method has been used in Ref. [92] to reduce the full amplitude to the different spin structures and perform the reduction to the master integrals. Using the method of Refs. [93, 94] it was not possible to achieve the reduction to master integrals. For the most complicated double-box topologies the reduction has been done only for a special ratio of  $m_t$  and the  $W$ -boson mass  $m_W$ . The relation

$$\frac{m_t^2}{m_W^2} \approx \frac{14}{3}$$

is used in Ref. [92]. Using this ratio, which is perfectly compatible with the recent measurements, the number of independent mass scales, which are treated algebraically in the reduction, is reduced by one. Using in addition the top-quark mass to set the mass scale for all dimensionful quantities, the number of scales is further reduced. These simplifications are crucial to simplify the algebraic complexity of the integral coefficients appearing in the Laporta reduction. As far as possible the results obtained with Reduze2 were checked with the aforementioned program Crusher. Further cross checks have been done using a private implementation of the Laporta algorithm making use of ICE [108] discussed in Sect. 6.3. Since the expression for the double-box topologies are very lengthy and the master integrals are still unknown the results are presented in Ref. [92] in form of a computer library. More precisely the contribution of the different master integrals  $MI_r$  to the functions  $f_i$  are expanded in the dimensional regulator  $\varepsilon = (4 - d)/2$ :

$$f_i = \sum_r \sum_{s=-5}^4 \varepsilon^s f_{i,r,s} MI_r. \quad (38)$$

The coefficients  $f_{i,r,s}$  are encoded in a C++ library.

## 5. Top-quark decay

So far, the only decay modes of the top quark which have been observed, i.e., semileptonic and non-leptonic decays with an intermediate  $W$  and a  $b$ -jet, result from  $t \rightarrow Wb$ . In the SM the branching ratio  $B(t \rightarrow Wb) \simeq 0.998$ , while those of the Cabibbo-suppressed modes, which have not yet been detected, are  $B(t \rightarrow Ws) \simeq$

$1.9 \times 10^{-3}$  and  $B(t \rightarrow Wd) \simeq 10^{-4}$ . For the dominant semileptonic and non-leptonic decay modes, the branching ratios are, including the order  $\alpha_s$  corrections ( $\ell = e, \mu, \tau$ ):

$$\begin{aligned} B(t \rightarrow b\ell^+\nu_\ell) &\simeq 0.108, \\ B(t \rightarrow bq\bar{q}') &\simeq 0.337 \times |V_{q\bar{q}'}|^2, \end{aligned} \quad (39)$$

where  $V_{q\bar{q}'}$  denotes a Cabibbo-Kobayashi-Maskawa (CKM) matrix element. At the differential level, polarized semileptonic and non-leptonic top-quark decays were analyzed to order  $\alpha_s$  in Ref. [109] and Ref. [53], respectively, while to order  $\alpha_s^2$  semileptonic top-quark decays have been recently investigated [110, 111].

### Polarized top-quark decay to $\ell\nu b$ -jet + jet

Gluon radiation can actually make up a fair fraction of the total top-quark decay rate if the gluon energy  $E_g$  is relatively low. For a gluon energy  $E_g \sim 10$  GeV the branching ratio  $B(t \rightarrow Wbg) \simeq 0.25$ . It is therefore of interest to analyze top-quark decays with an additional jet beyond LO QCD within the SM.

In Ref. [112] the decay of polarized top quarks to leptons, a  $b$ -jet and an additional jet was investigated at NLO QCD, at the differential level, for an off-shell intermediate  $W$  boson.

$$t \rightarrow W^{*+} + b \text{ jet} + \text{jet} \rightarrow \ell^+\nu_\ell + b \text{ jet} + \text{jet}, \quad (40)$$

Jets were defined by the Durham algorithm [113]. Soft and collinear singularities were handled by means of the dipole subtraction method [77]. The decay rate and a number of distributions were computed for different values of the jet resolution parameter  $Y$ . These include the energy distributions of the (non)  $b$ -flavored jet and of the charged lepton, the invariant mass distribution  $M_{b\ell}$  and the helicity angle  $\cos\theta_{W\ell}^*$ . Of interest are also the top-spin analyzing powers of the charged lepton and the  $b$ -jet and their dependence on  $Y$ . Examples are given in Tab. 13.

The results of Ref. [112] can be used as a building block for predictions of top-quark production and decay at NLO QCD, for instance for  $t\bar{t}$  + jet and single top + jet production.

### Anomalous form factors in $t \rightarrow Wb$

New interactions which affect the top quark can contribute to the  $t \rightarrow Wb$  decay amplitude and can cause deviations from the strength and V-A Lorentz structure of the tree-level SM amplitude. A model-independent analysis of the structure of this vertex can be made using a form-factor decomposition. The amplitude  $\mathcal{M}_{tbW}$  of the decay  $t(p) \rightarrow b(k) W^+(q)$ , where all particles are

Table 13: Top-spin analyzing powers of the charged lepton and the  $b$ -jet in the decay (40), for two different values of the jet resolution parameter  $Y$ .

	$Y = 0.01$	$Y = 0.001$
$\kappa_{\ell}^{\text{LO}}$	0.981	0.993
$\kappa_{\ell}^{\text{NLO}}$	0.983	0.996
$\kappa_b^{\text{LO}}$	-0.326	-0.368
$\kappa_b^{\text{NLO}}$	-0.319	-0.364

on-shell, can be decomposed in terms of four form factors:

$$\begin{aligned} \mathcal{M}_{tbW^+} = & -\frac{g_W}{\sqrt{2}} \epsilon^{\mu\nu} \bar{u}_b [(V_{tb}^* + f_L) \gamma_\mu P_L \\ & + f_R \gamma_\mu P_R + i\sigma_{\mu\nu} q^\nu (\frac{g_L}{m_W} P_L + \frac{g_R}{m_W} P_R)] u_t, \end{aligned} \quad (41)$$

with  $P_{L,R} = (1 \mp \gamma_5)/2$ . Here  $V_{tb}$  is the CKM matrix element in the three-generation SM, and  $p$ ,  $k$ , and  $q = p - k$  denote the four-momenta of the  $t$  and  $b$  quark and the  $W$  boson, respectively. The two chirality conserving and flipping form factors  $f_{L,R}$  and  $g_{L,R}$ , respectively, are dimensionless (complex) functions of  $q^2$ . If the  $W$  boson is off-shell, two additional form factors appear in the matrix element (41). However, they do not contribute to the matrix element of  $t \rightarrow b f_1 \bar{f}_2$  in the limit of vanishing fermion masses  $m_{f_{1,2}}$ .

The parameterization in (41) is chosen in such a way that non-zero values of  $f_{L,R}$  and  $g_{L,R}$  signify deviations from the structure of the tree-level Born vertex. Such deviations are generated both by SM loop corrections and, possibly, by new physics interactions. In the SM and in SM extensions which correspond to renormalizable theories,  $f_{L,R} \neq 0$  can appear at tree-level while  $g_{L,R} \neq 0$  must be loop-induced. In the following we use the convention that  $f_{L,R}$  and  $g_{L,R}$  parameterize only the new physics contributions to  $t \rightarrow bW$ . (In the framework of effective Lagrangians,  $f_{L,R}$  and  $g_{L,R}$  correspond to constant anomalous couplings.)

In Ref. [114] the form factors  $f_{L,R}$  and  $g_{L,R}$  were computed for a number of phenomenologically acceptable extensions of the Standard Model, namely a type-II non-supersymmetric 2-Higgs doublet extension (2HDM), the minimal supersymmetric extension (MSSM), a top-color assisted technicolor model (TC2) and, cursorily, a variant of the Little Higgs models. While in the 2HDM and the MSSM electroweak symmetry breaking (EWSB) is triggered by elementary Higgs fields, the latter two models are paradigms for the special role the top quark may play in the mechanism of EWSB. The magnitudes and phases of  $f_{L,R}$  and  $g_{L,R}$  were computed at 1-loop order. The results of this analysis are as follows.

The imaginary parts of the form factors, which can be induced either by  $CP$ -invariant final-state rescattering or by  $CP$ -violating interactions, are very small compared to the real parts. Moreover, within the above models,

$$|\text{Re}f_R|, |\text{Re}g_L| \ll |\text{Re}g_R| < |\text{Re}f_L|. \quad (42)$$

In the 2HDM and the MSSM, the magnitudes of the anomalous couplings  $f_L$ ,  $g_R$  are smaller than 1%. TC2 interactions can induce an anomalous form factor  $\text{Re}f_L$  as large as  $-0.06V_{tb}^*$ . This would reduce the top width by  $\sim 10\%$ . A reduction of similar size can happen in Little Higgs models.

Direct empirical information about the anomalous couplings  $f_R \simeq \text{Re}f_R$ ,  $g_R \simeq \text{Re}g_R$ , and  $g_L \simeq \text{Re}g_L$  is obtained from the measurement of the  $W$  helicity fractions

$$F_\lambda = \frac{\Gamma(t \rightarrow bW(\lambda))}{\Gamma(t \rightarrow bW)}, \quad \lambda = 0, \mp 1. \quad (43)$$

Comparison of the measured values of  $F_\lambda$  with the SM predictions, which are available to order  $\alpha_s^2$  [115], yields correlated bounds on these couplings. For recent results of the Tevatron and LHC experiments, see Refs. [116, 117, 118]. Strong bounds on  $f_L$ ,  $f_R$ , and  $g_R$  can be derived [119] from  $B(\bar{B} \rightarrow X_s \gamma)$ . The magnitudes of the anomalous form factors  $f_L$ ,  $f_R$ ,  $g_L$ , and  $g_R$  which were computed in Ref. [114] for the SM extensions mentioned above and found to be very small apart from  $f_L$ , are not in conflict with these bounds. The  $W$  helicity fractions do not provide information on the anomalous form factor  $f_L$ . In single-top-quark production at the LHC one may measure  $f_L$  with a precision of about 5%. The determination of the top width  $\Gamma_t$  with an accuracy of about 10% would require a high-energy  $e^+e^-$  (linear) collider where  $\Gamma_t$  could be obtained from fits to the precision measurement of the  $t\bar{t}$  production cross section at threshold.

In Ref. [120] polarized semileptonic top-quark decay  $t \rightarrow b\ell\nu_\ell(g)$  was considered at NLO QCD, assuming a small  $V + A$  admixture to the  $tWb$  vertex. It was analyzed how this admixture distorts energy and angular distributions.

## 6. Methods and tools

### 6.1. NNLO antenna subtraction method

The computation of differential distributions in higher order QCD requires a method to handle the infrared (IR) singularities (i.e. soft and collinear singularities) which appear in the individual contributions

to these distributions. At NNLO QCD, several methods have been developed. These include the sector decomposition algorithm [121, 122], the subtraction methods of [123], of Refs. [124, 125], Czakon’s method [126, 127, 128], which can be used for massless and massive partons, and the antenna subtraction method [129, 130, 131, 132].

In Refs. [133, 134, 135] the NNLO QCD subtraction terms were determined, within the antenna subtraction framework, for reactions of the type

$$S \rightarrow Q\bar{Q} + X, \quad (44)$$

where  $S$  denotes an uncolored initial state, for example, an  $e^+e^-$  pair or an uncolored boson, and  $Q$  is a massive quark. The antenna method was worked out in Refs. [136, 137] for QCD processes at NLO involving massive quarks. Partial results exist for NNLO QCD processes with colored initial states and massive quarks in the final state [138, 139, 140, 141]. Very recently, a NNLO QCD generalization of the phase-space slicing method has been presented by Refs. [142, 143] for  $e^+e^- \rightarrow \gamma^* \rightarrow Q\bar{Q}X$ .

To order  $\alpha_s^2$  the differential cross section of the reactions (44) is given, schematically, by

$$d\sigma = d\sigma_{\text{LO}} + d\sigma_{\text{NLO}} + d\sigma_{\text{NNLO}}. \quad (45)$$

The term  $d\sigma_{\text{NNLO}}$  receives the following contributions:

- i) the double virtual correction  $d\sigma_{\text{NNLO}}^{\text{VV}}$  associated with the second-order matrix element of  $S \rightarrow Q\bar{Q}$  (i.e., 2-loop times Born and 1-loop squared),
- ii) the real-virtual cross section  $d\sigma_{\text{NNLO}}^{\text{RV}}$  associated with the second-order matrix element of  $S \rightarrow Q\bar{Q}g$  (1-loop times Born),
- iii) the double real contribution  $d\sigma_{\text{NNLO}}^{\text{RR}}$  associated with the squared Born amplitudes  $S \rightarrow Q\bar{Q}gg$ ,  $S \rightarrow Q\bar{Q}q\bar{q}$  (where  $q$  denotes a massless quark), and above the  $4Q$  threshold,  $S \rightarrow Q\bar{Q}Q\bar{Q}$ . The latter contribution is IR finite and is of no concern for the purpose of constructing subtraction terms.

All the terms discussed below denote renormalized quantities. The ultraviolet divergences in the loop amplitudes are removed by on-shell renormalization of the external quarks and gluons – in the following,  $m_Q$  denotes the on-shell mass of  $Q$  – and by  $\overline{\text{MS}}$  renormalization of the strong coupling.

The terms i), ii), iii) are, apart from the  $Q\bar{Q}Q\bar{Q}$  contribution, separately IR divergent. In a generic subtraction

scheme,  $d\sigma_{\text{NNLO}}$  is given schematically by

$$\begin{aligned} d\sigma_{\text{NNLO}} = & \int_{\Phi_4} (d\sigma_{\text{NNLO}}^{\text{RR}} - d\sigma_{\text{NNLO}}^{\text{S}}) \\ & + \int_{\Phi_3} (d\sigma_{\text{NNLO}}^{\text{RV}} - d\sigma_{\text{NNLO}}^{\text{T}}) \\ & + \int_{\Phi_2} d\sigma_{\text{NNLO}}^{\text{VV}} + \int_{\Phi_3} d\sigma_{\text{NNLO}}^{\text{T}} + \int_{\Phi_4} d\sigma_{\text{NNLO}}^{\text{S}}. \end{aligned} \quad (46)$$

The subscripts  $\Phi_n$  denote  $n$ -particle phase-space integrals. Measurement functions are implicit in the integrands of the right-hand side of this equation. Here  $d\sigma_{\text{NNLO}}^{\text{S}}$  collectively denotes the double real subtraction terms for the  $Q\bar{Q}q\bar{q}$  and  $Q\bar{Q}gg$  matrix elements, and  $d\sigma_{\text{NNLO}}^{\text{T}}$  is real-virtual subtraction term for the  $Q\bar{Q}g$  matrix element. The subtraction terms  $d\sigma_{\text{NNLO}}^{\text{S}}$  are constructed such that

$$\begin{aligned} \int_{\Phi_4} [d\sigma_{\text{NNLO}}^{\text{RR}, Q\bar{Q}gg} - d\sigma_{\text{NNLO}}^{\text{S}, Q\bar{Q}gg}]_{\epsilon=0} & = \text{finite}, \\ \sum_q \int_{\Phi_4} [d\sigma_{\text{NNLO}}^{\text{RR}, Q\bar{Q}q\bar{q}} - d\sigma_{\text{NNLO}}^{\text{S}, Q\bar{Q}q\bar{q}}]_{\epsilon=0} & = \text{finite} \end{aligned} \quad (47)$$

in all single and double unresolved limits. The subtraction term  $d\sigma_{\text{NNLO}}^{\text{T}}$  must reproduce both the (implicit) singularities in single unresolved phase-space regions and the explicit poles of the real-virtual cross section  $d\sigma_{\text{NNLO}}^{\text{RV}}$ . The sum of the last three terms in (46) is then also IR finite. The integrals of these subtraction terms, denoted by  $\int_{\Phi_3} d\sigma_{\text{NNLO}}^{\text{T}}$  and  $\int_{\Phi_4} d\sigma_{\text{NNLO}}^{\text{S}}$  in (46), must be computed over the phase-space regions where IR singularities arise. Then the cancellation of IR singularities in (46) is made explicit.

In the antenna subtraction formalism, the subtraction terms are constructed from antenna functions and reduced matrix elements with remapped momenta. The antenna functions are *universal building blocks* and can be derived from the respective physical color-ordered squared matrix elements. For the reactions (44) the unintegrated and integrated NNLO antenna functions for the  $Q\bar{Q}q\bar{q}$  and  $Q\bar{Q}gg$  final states were computed in Ref. [133] and in Ref. [134], respectively, and for the  $Q\bar{Q}g$  final state in Ref. [135]. For definiteness, the antenna functions were determined by choosing in (44) the initial state  $S = \gamma^*$ . The main technical challenge is the analytic calculation of the integrated antenna functions, i.e.,  $\int_{\Phi_3} d\sigma_{\text{NNLO}}^{\text{T}}$  and  $\int_{\Phi_4} d\sigma_{\text{NNLO}}^{\text{S}}$  in  $d \neq 4$  dimensions.

Using the respective color-ordered squared matrix elements of the  $Q\bar{Q}q\bar{q}$  and  $Q\bar{Q}gg$  final state, the integrated 4-particle antenna functions were computed as follows. The  $d$ -dimensional 4-particle phase-space measure was represented in terms of cut propagators [144]. With the computer implementation FIRE [145] and AIR [146] of the integration-by-parts reduction and the Laporta algorithm, the integrated antenna functions were expressed

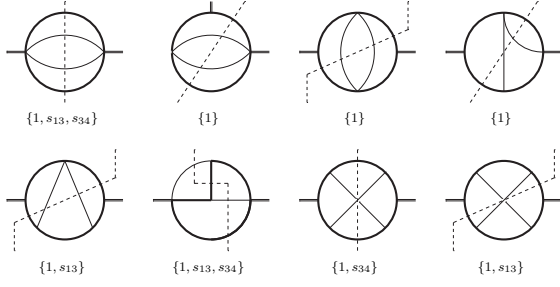


Figure 18: The 8 topologies corresponding to the 15 master integrals which determine the integrated antenna functions for the  $Q\bar{Q}q\bar{q}$  and  $Q\bar{Q}gg$  final states. Bold (thin) lines refer to massive (massless) scalar propagators. The dashed lines represent 4-particle cuts. The external line represents the external off-shell momentum  $q$ . The terms  $s_{ij} = 2p_i \cdot p_j$  in the curly brackets below each topology denote additional factors in the corresponding integrand of the 4-particle phase-space integral.

in terms of a set of 15 scalar master integrals involving  $d$ -dimensional 4-particle integration, see Fig. 18. These master integrals were computed, in  $d = 4 - 2\epsilon$  dimensions by Laurent expansion in  $\epsilon$ , using the differential-equations method [147, 148]. The integration constants were fixed by computing the master integrals at threshold  $q^2 = 4m^2$ . These master integrals can be expressed in terms of harmonic polylogarithms (HPL) [149] in the variable  $y = (1 - \beta)/(1 + \beta)$ , where  $\beta = \sqrt{1 - 4m_Q^2/s}$ .

The leading and subleading color NNLO integrated antenna functions for the  $Q\bar{Q}g$  final state were computed in analogous fashion [135]. They can be expressed in terms of 22 master integrals which correspond to three-particle cuts through three-loop scalar self-energy type Feynman integrals, involving massive and massless scalar propagators, see Fig. 19. These master integrals were also computed with the differential-equations method. Master integrals associated with 6 topologies can be expressed in terms of HPL with argument  $y$  up to and including weight four. Master integrals with the remaining 5 topologies are given in terms of cyclotomic harmonic polylogarithms which were analyzed in detail in Refs. [150, 151, 152, 153, 154].

As a check of these integrated double-real and real-virtual subtraction terms, the second order contribution  $R^{(2)}$  to the ratio  $R_Q(s)$  defined by

$$\begin{aligned} R_Q(s) &= \frac{\sigma(e^+ e^- \rightarrow \gamma^* \rightarrow Q\bar{Q} + X)}{\sigma(e^+ e^- \rightarrow \gamma^* \rightarrow \mu^+ \mu^-)} \\ &= R^{(0)} + \left(\frac{\alpha_s(\mu^2)}{2\pi}\right) R^{(1)} + \left(\frac{\alpha_s(\mu^2)}{2\pi}\right)^2 R^{(2)} \end{aligned}$$

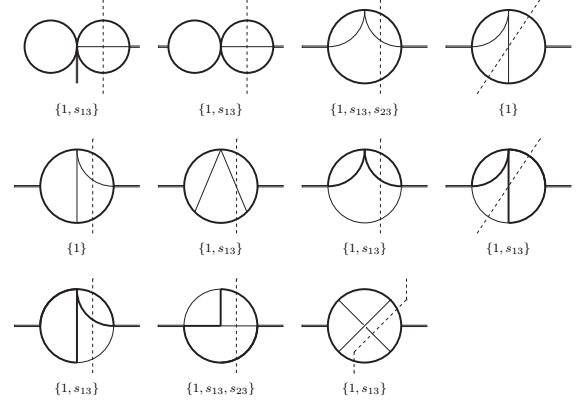


Figure 19: The 11 topologies corresponding to the 22 master integrals which determine the integrated antenna functions for the  $Q\bar{Q}g$  final state. The notation follows Fig. 18. The terms in the curly brackets below each topology denote additional factors in the corresponding integrand of the combined phase-space and loop integral.

$$+O(\alpha_s^3) \quad (48)$$

was computed in Ref. [135] and compared with results in the literature. The NLO correction has been known for a long time [155]. The second order contribution may be decomposed as follows:

$$\begin{aligned} R^{(2)} &= e_Q^2 (N_c^2 - 1) \left( N_c R_{\text{LC}}^{(2)} - \frac{1}{N_c} R_{\text{SC}}^{(2)} \right. \\ &\quad \left. + n_f R_f^{(2)} + R_F^{(2)} \right). \end{aligned} \quad (49)$$

Computing  $R^{(2)}$  from the contributions of the individual final states requires the integrated NNLO 4- and 3-particle antenna subtraction terms discussed above, the NNLO QCD matrix element  $\gamma^* \rightarrow Q\bar{Q}$  [156] and, above the  $Q\bar{Q}Q\bar{Q}$  threshold, the matrix element  $\gamma^* \rightarrow Q\bar{Q}Q\bar{Q}$ , which is UV and IR finite. The analytic computation of  $R_f^{(2)}$  of Ref. [133] agrees with the result of Ref. [157].

The leading and subleading color contributions  $R_{\text{LC}}^{(2)}$ ,  $R_{\text{SC}}^{(2)}$  were known in the literature in analytic fashion only i) near the  $Q\bar{Q}$  threshold as an expansion in  $\beta$  up to and including terms of order  $\beta$  [158] (cf. also Ref. [159]) and ii) in the high-energy limit  $x = m_Q^2/s \rightarrow 0$  as asymptotic expansions in  $x$  up to and including terms of order  $x^6$  [160]. Using the threshold and asymptotic expansions, Ref. [161] determined  $R_{\text{LC}}^{(2)}$  and  $R_{\text{SC}}^{(2)}$  in the intermediate energy range  $0 < \beta \leq 1$  by Padé approximation. For comparison with the threshold and asymptotic expansions known in the literature, we use

$$\begin{aligned} R_{\text{NA}}^{(2)} &= \frac{N_c}{2} (R_{\text{LC}}^{(2)} - R_{\text{SC}}^{(2)}), \\ R_{\text{A}}^{(2)} &= N_c R_{\text{SC}}^{(2)}. \end{aligned} \quad (50)$$

The calculation of these functions in Ref. [135], shown in Fig. 20 is exact in the whole physical region and

agrees with these previous results. In particular, the threshold expansion of  $R^{(2)}$  can be obtained analytically [162], beyond the terms known so far. This is of interest for the investigation of  $e^+e^- \rightarrow t\bar{t}X$  near threshold.

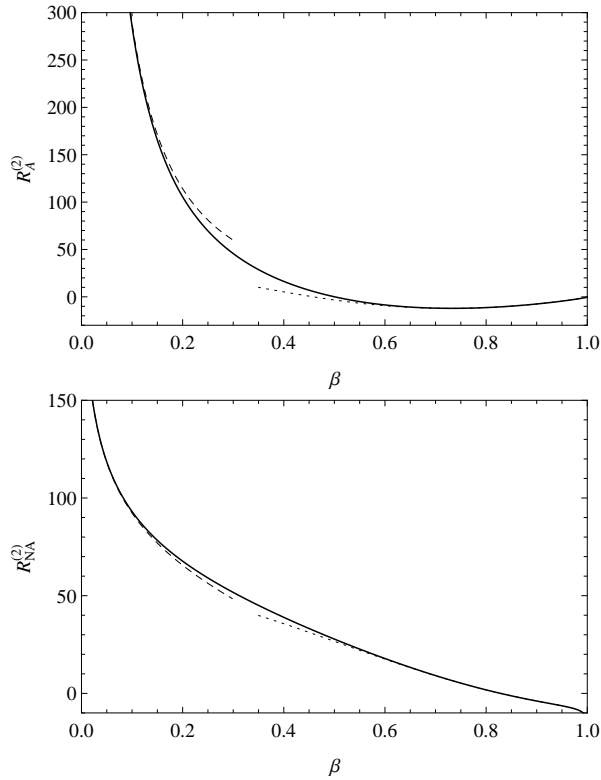


Figure 20: The function  $R_A^{(2)}$  (upper plot) and  $R_{NA}^{(2)}$  (lower plot) defined in (50). The solid lines are the exact results [135], the dashed and dotted lines are the threshold and asymptotic expansions from [158] and [160], respectively.

### Two-loop vertex functions

The computation of differential distributions at NNLO QCD for reactions of the type (44) requires, apart from the subtraction terms discussed above, of course also the matrix elements of the individual contributions to this order of perturbation theory. The renormalized NNLO QCD matrix elements for  $J \rightarrow Q\bar{Q}$ , where  $J$  denotes a color-singlet current, were computed in Refs. [156, 163, 164, 165] for  $J =$  vector current, non-singlet and singlet axial vector current, and scalar and pseudo-scalar current, respectively. As a by-product of these computations, the anomalous magnetic moments, weak magnetic moments and axial charges of the top and bottom quark were computed to order  $\alpha_s^2$  in Ref. [166]. The leading terms in  $\beta$  of the order  $\alpha_s^2$  cross section for  $e^+e^- \rightarrow \gamma^*, Z^* \rightarrow Q\bar{Q}X$  in the vicinity

of the production threshold where the  $Q\bar{Q}$  contribution dominates, were determined in Ref. [167].

An important observable is the forward-backward asymmetry  $A_{FB}^Q$  in heavy quark-pair production in  $e^+e^- \rightarrow \gamma^*, Z^* \rightarrow Q\bar{Q}X$ ,  $Q = b, t$ . It was computed to order  $\alpha_s^2$  for massless quarks in Ref. [168]. As is well-known, for  $b$  quarks produced at the  $Z$  resonance, there is some tension between the measured forward-backward asymmetry and the SM result. For massless quarks  $Q$ , the  $Q\bar{Q}$  contribution to  $A_{FB}^Q$  resulting from the interference of the vector and non-singlet axial vector matrix elements is zero in QCD. (The ‘anomaly contribution’, which results from the interference of the vector and singlet axial vector matrix elements, is IR finite and very small.) In Ref. [169] the  $Q\bar{Q}$  contributions to  $A_{FB}^Q$  were computed to order  $\alpha_s^2$  for massive quarks. These contributions are IR finite. The order  $\alpha_s^2$  contributions of the  $Q\bar{Q}g$  and  $Q\bar{Q}gg$ ,  $Q\bar{Q}q\bar{q}$  final states to  $A_{FB}^Q$  were calculated, for  $b$  quarks at the  $Z$  resonance and for  $t\bar{t}$  production above threshold, in Ref. [170]. The IR singularities, which appear in the 3-parton and 4-parton contributions to the asymmetry at this order of perturbation theory, can be handled with NLO dipole subtraction terms [77]. The resulting  $A_{FB}^b$  at the  $Z$  resonance was found to be slightly smaller [170] than the corresponding result for massless quarks [168]. This can be understood from the fact that a massive (anti)quark is more inert than a massless one in radiating off partons and, hence, changes its direction less likely with respect to the leading-order  $Q\bar{Q}$  configuration.

### 6.2. AutoDipole — Automatic generation of Catani-Seymour subtraction terms

Beyond leading order, virtual corrections as well as real corrections need to be considered. Only the sum of the two yields an infrared finite result. While in the virtual corrections, i.e., after loop integration, the soft and collinear singularities are manifest, in the real corrections the singularities are manifest only after the phase-space integration has been carried out. Using dimensional regularization requires to perform the phase-space integration in  $d$  space time dimensions. Given the complicated structure of the phase space and the matrix elements and taking into account the experimental cuts, such an integration is highly non-trivial. With the Catani-Seymour subtraction method an algorithmic solution has been proposed [76, 77]. The main idea is to add and subtract local counter-terms in order to render virtual corrections and real corrections individually finite. For a  $n$ -parton final state the method reads:

$$\delta\sigma_n^{\text{NLO}} = \int dR_n d\sigma_n^V + \int dR_{n+1} d\sigma_{n+1}^R$$

$$\begin{aligned}
&= \int dR_n (d\sigma_n^V + \int d\Phi A) \\
&+ \int dR_{n+1} (d\sigma_{n+1}^R - A). \quad (51)
\end{aligned}$$

Here,  $d\sigma_n^V$  ( $d\sigma_{n+1}^R$ ) denotes the differential cross section for the virtual (real) corrections, which has to be integrated over the  $n$  ( $n + 1$ ) parton final state in order to obtain the contribution to the total cross section. The  $n + 1$  parton phase-space measure is factorized into an unresolved ( $d\Phi$ ) and resolved contribution ( $dR_n$ ):  $dR_{n+1} = dR_n \times d\Phi$ . A local counter-term  $A$  is constructed such that the combination  $(d\sigma_{n+1}^R - A)$  is finite for all single unresolved contributions (one parton soft or two partons collinear). Furthermore, the subtraction term  $A$  is chosen so that  $\int d\Phi A$  can be calculated analytically to cancel the divergencies in the virtual corrections. In Refs. [76, 77] an explicit representation of the subtraction term as sum over so-called dipoles is given:

$$A = \sum_{i,j,k} \mathcal{D}_{ij,k}, \quad (52)$$

where the sum is over the collinear particles ( $i, j$ ) and a spectator parton ( $k$ ). Each dipole is calculated from process independent functions (capturing the universal properties of the singular limits), sandwiched between process specific amplitudes. While in principle the evaluation is straightforward, the calculation of the dipoles is tedious and error-prone: First of all, for high multiplicities, a large number of dipoles needs to be considered. For example, for the reaction  $gg \rightarrow t\bar{t}g$  considered in Sect. 3, 36 dipoles had to be calculated. Furthermore, for each dipole, the specific factorization of the phase-space measure, leading to a reduced  $n$ -parton kinematics, needs to be evaluated. In addition, non-trivial color correlations and spin-correlations have to be determined. It is also worth noting that the evaluation of a large number of dipoles during the numerical integration can be rather time-consuming. The numerical computation of the dipoles may take even longer than the calculation of the matrix element for the corresponding real corrections. An efficient implementation is thus mandatory to reduce the computational costs. While in Refs. [14, 15] a private C++ library has been developed, in which the dipoles are built-up using the library functions, a different approach was used in the publicly available AutoDipole package in Ref. [171]. A mathematica library is provided which acts as code generator. After having specified the process, a Fortran source code is generated for the calculation of the subtraction terms. In addition also code is created for testing the collinear and soft limits. The color correlated

matrix elements are calculated by interfacing the Madgraph library [75]. The AutoDipole package has been tested for various  $2 \rightarrow 5$  and  $2 \rightarrow 6$  processes.

In Ref. [172] the implementation has been extended to allow also the computation of dipole subtraction terms in the MSSM.

### 6.3. ICE – the IBP Chooser of Equations

A major bottleneck in the evaluation of higher order corrections in quantum field theory—besides the evaluation of the master integrals—is the reduction of multi-loop tensor integrals to the master integrals. While different approaches exist (see also the discussion in Sect. 4) most techniques rely sooner or later on the application of IBP and Lorentz invariance (LI) [148] equations. For simple problems these equations can be rearranged manually by inspection to implement a reduction scheme. For complicated topologies, e.g. double-box topologies, this task is very cumbersome. An alternative approach is given by the Laporta algorithm where the IBP and LI equations, valid formally for arbitrary space-time dimensions and arbitrary powers of the propagators, are specified by setting the powers of the propagators to integer values. Using different seeds for the integer values a large system of equations is constructed, which is then solved using a Gauss type elimination procedure. The limiting factors of this procedure are the number of equations and the size of the integral coefficients in the IBP equations. The latter are rational functions of the kinematical invariants and the space-time dimension. The simplifications of these coefficients is typically done by the program Fermat [173]. In practical applications it turns out that a significant number of equations generated with the Laporta approach does not provide independent information. However, these equations can lead to a tremendous increase of algebraic complexity. Removing these equations at an early stage of the reduction could thus speed up the procedure. In Ref. [108] a method to remove dependent equations from the reduction procedure has been investigated. The basic idea is to use integer values for the kinematic invariants as well as for the space-time dimension. In a next step a Gauss elimination of this system is done and the linearly dependent equations are identified. Since the integral coefficients are now just numbers, no time-consuming algebraic manipulation of multivariate rational functions is required. The reduction is thus much faster than the reduction of the original problem. After having identified the dependent equations they are removed from the IBP system and the full reduction is started. In fact the procedure can be further optimized by a clever choice of the equations which are kept in the

Topology	Dots	Equations	Independent Equations	Ratio
H	1	10464	5767	0.55
H	2	39600	18626	0.47
BM	3	3114	1148	0.37
BM	10	113571	28851	0.25

Table 14: Number of equations before and after the application of the ICE algorithm [108].

system. As an example the topologies shown in Fig. 21 are studied in Ref. [108]. In Tab. 14 the number of inde-

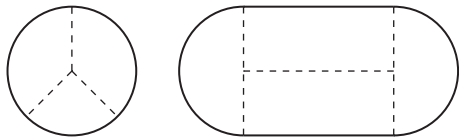


Figure 21: The three- and four-loop vacuum topologies BM (left) and H (right). The solid lines are massive, the dashed are massless. The names follow the notations in Refs. [174, 175, 176, 177].

pendent equations after the application of the ICE algorithm is shown together with the number of equations at the beginning. The complexity of the reduction is controlled by increasing the powers of the propagators. The additional propagators are quoted in Tab. 14 as *dots*. Already for simple cases about 50% of the IBP equations generated with the Laporta algorithm are not independent and can thus be removed from the reduction. For the BM topology with 10 dots, only a quarter of the IBP equations is independent and needs to be considered in the subsequent reduction. Using integer values for the kinematic invariants, it is in principle possible that an IBP equation becomes linearly dependent despite being independent for a general kinematics. However, it has been shown in Ref. [108] that the probability of failure can be made very low by a clever choice of the integer values. In particular, choosing the integer values modulo a large prime  $p$  the probability to correctly identify the independent equations is given by

$$P(\text{success}) \geq \prod_{i=1}^r \left(1 - \frac{i}{p}\right) \quad (53)$$

where  $r$  denotes the rank of the linear system. For large prime numbers the probability of failure can thus be made very low. Note that in case the ICE algorithm fails, no false equations are generated. It just means that an equation which is independent is accidentally removed from the system. In the worst case this would just mean that the reduction to master integrals in the subsequent Laporta step is incomplete. Very recently

the ICE algorithm has been applied in a private implementation of the Laporta algorithm [178]. Using ICE a significant improvement of the runtime can be observed.

## 7. Summary

This project had a strong focus on hadron collider phenomenology. Quite a number of predictions on hadronic  $t\bar{t}$  and  $t\bar{t} + 1$ -jet production, including top-quark decay, which were made within the Standard Model at NLO in the QCD and weak couplings were confronted with data from the Tevatron and the LHC. Overall the agreement between SM theory and experiment is, so far, very good. These results contributed to our present understanding of the properties and interactions of the top quark. They will remain relevant also for the analysis and interpretation of future LHC data on top-quark production and decay.

## Acknowledgments

We would like to thank M. Assadsolimani, B. Biedermann, C. Bogner, A. Brandenburg, K. Bzheumikova, O. Dekkers, M. Fücker, P. Galler, T. Gehrmann, P. Gonzalez, K. Hasegawa, R. Heinesch, D. Heisler, P. Kant, U. Langenfeld, T. Leineweber, E. Matiske, T. Martini, C. Mellein, C. Meyer, S. Mölbitz, S. Schade, Z.-G. Si, T. Sult, B. Tausk, J. Usovitsch, K. Waninger, and M. Wiebusch who have contributed over the years to projects reviewed in this article.

## References

- [1] F. Abe, et al., Observation of top quark production in  $\bar{p}p$  collisions, Phys.Rev.Lett. 74 (1995) 2626–2631, arXiv:hep-ex/9503002, doi:10.1103/PhysRevLett.74.2626.
- [2] S. Abachi, et al., Observation of the top quark, Phys.Rev.Lett. 74 (1995) 2632–2637, arXiv:hep-ex/9503003, doi:10.1103/PhysRevLett.74.2632.
- [3] D. Chakraborty, Top quark and W/Z results from the Tevatron, arXiv:hep-ex/0212027.
- [4] V. Abazov, et al., Evidence for production of single top quarks and first direct measurement of  $V_{tb}$ , Phys.Rev.Lett. 98 (2007) 181802, arXiv:hep-ex/0612052, doi:10.1103/PhysRevLett.98.181802.

- [5] P. Nason, S. Dawson, R. K. Ellis, The Total Cross-Section for the Production of Heavy Quarks in Hadronic Collisions, *Nucl.Phys.* B303 (1988) 607, doi:10.1016/0550-3213(88)90422-1.
- [6] W. Beenakker, H. Kuijf, W. van Neerven, J. Smith, QCD Corrections to Heavy Quark Production in  $p$  anti- $p$  Collisions, *Phys.Rev.* D40 (1989) 54–82, doi:10.1103/PhysRevD.40.54.
- [7] W. Beenakker, W. van Neerven, R. Meng, G. Schuler, J. Smith, QCD corrections to heavy quark production in hadron hadron collisions, *Nucl.Phys.* B351 (1991) 507–560, doi:10.1016/S0550-3213(05)80032-X.
- [8] W. Bernreuther, A. Brandenburg, Z. Si, P. Uwer, Top quark spin correlations at hadron colliders: Predictions at next-to-leading order QCD, *Phys.Rev.Lett.* 87 (2001) 242002, arXiv:hep-ph/0107086, doi:10.1103/PhysRevLett.87.242002.
- [9] G. Bordes, B. van Eijk, Calculating QCD Corrections to Single Top Production in Hadronic Interactions, *Nucl. Phys.* B435 (1995) 23–58, doi:10.1016/0550-3213(94)00460-V.
- [10] T. Stelzer, Z. Sullivan, S. Willenbrock, Single Top Quark Production via W-Gluon Fusion at Next-To-Leading Order, *Phys. Rev.* D56 (1997) 5919–5927, arXiv:hep-ph/9705398, doi:10.1103/PhysRevD.56.5919.
- [11] B. Harris, E. Laenen, L. Phaf, Z. Sullivan, S. Weinzierl, The Fully Differential Single Top Quark Cross-Section in Next to Leading Order QCD, *Phys. Rev.* D66 (2002) 054024, arXiv:hep-ph/0207055, doi:10.1103/PhysRevD.66.054024.
- [12] S. Moch, P. Uwer, Theoretical status and prospects for top-quark pair production at hadron colliders, *Phys.Rev.* D78 (2008) 034003, arXiv:0804.1476, doi:10.1103/PhysRevD.78.034003.
- [13] R. Bonciani, S. Catani, M. L. Mangano, P. Nason, NLL resummation of the heavy quark hadroproduction cross-section, *Nucl.Phys.* B529 (1998) 424–450, arXiv:hep-ph/9801375, doi:10.1016/j.nuclphysb.2008.06.006, doi:10.1016/S0550-3213(98)00335-6.
- [14] S. Dittmaier, P. Uwer, S. Weinzierl, NLO QCD corrections to  $t$  anti- $t$  + jet production at hadron colliders, *Phys.Rev.Lett.* 98 (2007) 262002, arXiv:hep-ph/0703120, doi:10.1103/PhysRevLett.98.262002.
- [15] S. Dittmaier, P. Uwer, S. Weinzierl, Hadronic top-quark pair production in association with a hard jet at next-to-leading order QCD: Phenomenological studies for the Tevatron and the LHC, *Eur.Phys.J.* C59 (2009) 625–646, arXiv:0810.0452, doi:10.1140/epjc/s10052-008-0816-y.
- [16] P. Bärnreuther, M. Czakon, A. Mitov, Percent Level Precision Physics at the Tevatron: First Genuine NNLO QCD Corrections to  $q\bar{q} \rightarrow t\bar{t} + X$ , *Phys.Rev.Lett.* 109 (2012) 132001, arXiv:1204.5201, doi:10.1103/PhysRevLett.109.132001.
- [17] M. Czakon, A. Mitov, NNLO corrections to top-pair production at hadron colliders: the all-fermionic scattering channels, *JHEP* 1212 (2012) 054, arXiv:1207.0236, doi:10.1007/JHEP12(2012)054.
- [18] M. Czakon, A. Mitov, NNLO corrections to top pair production at hadron colliders: the quark-gluon reaction, *JHEP* 1301 (2013) 080, arXiv:1210.6832, doi:10.1007/JHEP01(2013)080.
- [19] M. Czakon, P. Fiedler, A. Mitov, Total Top-Quark Pair-Production Cross Section at Hadron Colliders Through  $O(\alpha_s^4)$ , *Phys.Rev.Lett.* 110 (2013) 252004, arXiv:1303.6254, doi:10.1103/PhysRevLett.110.252004.
- [20] M. Czakon, A. Mitov, Top++: A Program for the Calculation of the Top-Pair Cross-Section at Hadron Colliders, *Comput.Phys.Commun.* 185 (2014) 2930, arXiv:1112.5675, doi:10.1016/j.cpc.2014.06.021.
- [21] M. Aliev, H. Lacker, U. Langenfeld, S. Moch, P. Uwer, et al., HATHOR: HAdronic Top and Heavy quarks crOss section calculatoR, *Comput.Phys.Commun.* 182 (2011) 1034–1046, arXiv:1007.1327, doi:10.1016/j.cpc.2010.12.040.
- [22] Y. Kiyo, J. H. Kühn, S. Moch, M. Steinhauser, P. Uwer, Top-quark pair production near threshold at LHC, *Eur.Phys.J.* C60 (2009) 375–386, arXiv:0812.0919, doi:10.1140/epjc/s10052-009-0892-7.
- [23] J. H. Kühn, E. Mirkes, QCD corrections to toponium production at hadron colliders, *Phys.Rev.* D48 (1993) 179–189, arXiv:hep-ph/9301204, doi:10.1103/PhysRevD.48.179.
- [24] A. Petrelli, M. Cacciari, M. Greco, F. Maltoni, M. L. Mangano, NLO production and decay of quarkonium, *Nucl.Phys.* B514 (1998) 245–309, arXiv:hep-ph/9707223, doi:10.1016/S0550-3213(97)00801-8.
- [25] M. Beneke, A. Signer, V. A. Smirnov, Top quark production near threshold and the top quark mass, *Phys.Lett.* B454 (1999) 137–146, arXiv:hep-ph/9903260, doi:10.1016/S0370-2693(99)00343-3.
- [26] A. Pineda, A. Signer, Heavy Quark Pair Production near Threshold with Potential Non-Relativistic QCD, *Nucl.Phys.* B762 (2007) 67–94, arXiv:hep-ph/0607239, doi:10.1016/j.nuclphysb.2006.09.025.
- [27] W. Beenakker, A. Denner, W. Hollik, R. Mertig, T. Sack, et al., Electroweak one loop contributions to top pair production in hadron colliders, *Nucl.Phys.* B411 (1994) 343–380, doi:10.1016/0550-3213(94)90454-5.
- [28] W. Bernreuther, M. Fuecker, Z. Si, Mixed QCD and weak corrections to top quark pair production at hadron colliders, *Phys.Lett.* B633 (2006) 54–60, arXiv:hep-ph/0508091, doi:10.1016/j.physletb.2005.11.056.
- [29] J. H. Kühn, A. Scharf, P. Uwer, Electroweak corrections to top-quark pair production in quark-antiquark annihilation, *Eur.Phys.J.* C45 (2006) 139–150, arXiv:hep-ph/0508092, doi:10.1140/epjc/s2005-02423-6.
- [30] W. Bernreuther, M. Fuecker, Z.-G. Si, Weak interaction corrections to hadronic top quark pair production, *Phys.Rev.* D74 (2006) 113005, arXiv:hep-ph/0610334, doi:10.1103/PhysRevD.74.113005.
- [31] J. H. Kühn, A. Scharf, P. Uwer, Electroweak effects in top-quark pair production at hadron colliders, *Eur.Phys.J.* C51 (2007) 37–53, arXiv:hep-ph/0610335, doi:10.1140/epjc/s10052-007-0275-x.
- [32] W. Bernreuther, M. Fuecker, Z.-G. Si, Weak interaction corrections to hadronic top quark pair production: Contributions from quark-gluon and  $b$  anti- $b$  induced reactions, *Phys.Rev.* D78 (2008) 017503, arXiv:0804.1237, doi:10.1103/PhysRevD.78.017503.
- [33] J. Kühn, A. Scharf, P. Uwer, Weak interactions in top-quark pair production at hadron colliders: An update, to appear in *Phys.Rev.D*, arXiv:1305.5773.
- [34] U. Langenfeld, S. Moch, P. Uwer, Measuring the running top-quark mass, *Phys.Rev.* D80 (2009) 054009, arXiv:0906.5273, doi:10.1103/PhysRevD.80.054009.
- [35] V. Abazov, et al., Combination of  $t$  anti- $t$  cross section measurements and constraints on the mass of the top quark and its decays into charged Higgs bosons, *Phys.Rev.* D80 (2009) 071102, arXiv:0903.5525, doi:10.1103/PhysRevD.80.071102.
- [36] J. H. Kühn, G. Rodrigo, Charge asymmetry of heavy quarks at hadron colliders, *Phys.Rev.* D59 (1999) 054017, arXiv:hep-ph/9807420, doi:10.1103/PhysRevD.59.054017.
- [37] W. Bernreuther, Z.-G. Si, Distributions and correlations for top quark pair production and decay at the Tevatron and LHC., *Nucl.Phys.* B837 (2010) 90–121, arXiv:1003.3926, doi:10.1016/j.nuclphysb.2010.05.001.
- [38] W. Hollik, D. Pagani, The electroweak contribution to the top quark forward-backward asymmetry at the Teva-

- tron, Phys.Rev. D84 (2011) 093003, arXiv:1107.2606, doi:10.1103/PhysRevD.84.093003.
- [39] J. Aguilar-Saavedra, D. Amidei, A. Juste, M. Perez-Victoria, Asymmetries in top quark pair production, arXiv:1406.1798.
- [40] V. Ahrens, A. Ferroglia, M. Neubert, B. D. Pecjak, L. L. Yang, The top-pair forward-backward asymmetry beyond NLO, Phys.Rev. D84 (2011) 074004, arXiv:1106.6051, doi:10.1103/PhysRevD.84.074004.
- [41] J. H. Kühn, G. Rodrigo, Charge asymmetries of top quarks at hadron colliders revisited, JHEP 1201 (2012) 063, arXiv:1109.6830, doi:10.1007/JHEP01(2012)063.
- [42] W. Bernreuther, Z.-G. Si, Top quark and leptonic charge asymmetries for the Tevatron and LHC, Phys.Rev. D86 (2012) 034026, arXiv:1205.6580, doi:10.1103/PhysRevD.86.034026.
- [43] M. Czakon, P. Fiedler, A. Mitov, Resolving the Tevatron top quark forward-backward asymmetry puzzle, arXiv:1411.3007.
- [44] J. Aguilar-Saavedra, W. Bernreuther, Z. Si, Collider-independent top quark forward-backward asymmetries: standard model predictions, Phys.Rev. D86 (2012) 115020, arXiv:1209.6352, doi:10.1103/PhysRevD.86.115020.
- [45] T. Aaltonen, et al., Measurement of the top quark forward-backward production asymmetry and its dependence on event kinematic properties, Phys.Rev. D87 (9) (2013) 092002, arXiv:1211.1003, doi:10.1103/PhysRevD.87.092002.
- [46] V. M. Abazov, et al., Measurement of the forward-backward asymmetry in top quark-antiquark production in ppbar collisions using the lepton+jets channel, arXiv:1405.0421.
- [47] S. Chatrchyan, et al., Measurements of the  $t\bar{t}$  charge asymmetry using the dilepton decay channel in pp collisions at  $\sqrt{s} = 7$  TeV, JHEP 1404 (2014) 191, arXiv:1402.3803, doi:10.1007/JHEP04(2014)191.
- [48] CMS Collaboration, Measurement of the  $t\bar{t}$  charge asymmetry with lepton+jets events at 8 TeV, CMS-PAS-TOP-12-033.
- [49] G. Aad, et al., Measurement of the top quark pair production charge asymmetry in proton-proton collisions at  $\sqrt{s} = 7$  TeV using the ATLAS detector, JHEP 1402 (2014) 107, arXiv:1311.6724, doi:10.1007/JHEP02(2014)107.
- [50] A. Chapelain, Charge asymmetry of top quark-antiquark pairs, arXiv:1401.6836.
- [51] V. Sharyy, Experimental status of top charge asymmetry measurements, arXiv:1312.0383.
- [52] W. Bernreuther, A. Brandenburg, Z. Si, P. Uwer, Top quark pair production and decay at hadron colliders, Nucl.Phys. B690 (2004) 81–137, arXiv:hep-ph/0403035, doi:10.1016/j.nuclphysb.2004.04.019.
- [53] A. Brandenburg, Z. Si, P. Uwer, QCD corrected spin analyzing power of jets in decays of polarized top quarks, Phys.Lett. B539 (2002) 235–241, arXiv:hep-ph/0205023, doi:10.1016/S0370-2693(02)02098-1.
- [54] G. Mahlon, S. J. Parke, Maximizing spin correlations in top quark pair production at the Tevatron, Phys.Lett. B411 (1997) 173–179, arXiv:hep-ph/9706304, doi:10.1016/S0370-2693(97)00987-8.
- [55] P. Uwer, Maximizing the spin correlation of top quark pairs produced at the Large Hadron Collider, Phys.Lett. B609 (2005) 271–276, arXiv:hep-ph/0412097, doi:10.1016/j.physletb.2005.01.005.
- [56] W. Bernreuther, M. Flesch, P. Haberl, Signatures of Higgs bosons in the top quark decay channel at hadron colliders, Phys.Rev. D58 (1998) 114031, arXiv:hep-ph/9709284, doi:10.1103/PhysRevD.58.114031.
- [57] W. Bernreuther, Z.-G. Si, Top quark spin correlations and polarization at the LHC: standard model predictions and effects of anomalous top chromo moments, Phys.Lett. B725 (1-3) (2013) 115–122, arXiv:1305.2066, doi:10.1016/j.physletb.2013.06.051.
- [58] G. Aad, et al., Measurement of Top Quark Polarization in Top-Antitop Events from Proton-Proton Collisions at  $\sqrt{s} = 7$  TeV Using the ATLAS Detector, Phys.Rev.Lett. 111 (23) (2013) 232002, arXiv:1307.6511, doi:10.1103/PhysRevLett.111.232002.
- [59] S. Chatrchyan, et al., Measurements of  $t\bar{t}$  spin correlations and top-quark polarization using dilepton final states in pp collisions at  $\sqrt{s} = 7$  TeV, Phys.Rev.Lett. 112 (2014) 182001, arXiv:1311.3924, doi:10.1103/PhysRevLett.112.182001.
- [60] W. Bernreuther, A. Brandenburg, P. Uwer, Transverse polarization of top quark pairs at the Tevatron and the large hadron collider, Phys.Lett. B368 (1996) 153–162, arXiv:hep-ph/9510300, doi:10.1016/0370-2693(95)01475-6.
- [61] V. M. Abazov, et al., Evidence for spin correlation in  $t\bar{t}$  production, Phys.Rev.Lett. 108 (2012) 032004, arXiv:1110.4194, doi:10.1103/PhysRevLett.108.032004.
- [62] G. Aad, et al., Observation of spin correlation in  $t\bar{t}$  events from pp collisions at  $\sqrt{s} = 7$  TeV using the ATLAS detector, Phys.Rev.Lett. 108 (2012) 212001, arXiv:1203.4081, doi:10.1103/PhysRevLett.108.212001.
- [63] G. Aad, et al., Measurements of spin correlation in top-antitop quark events from proton-proton collisions at  $\sqrt{s} = 7$  TeV using the ATLAS detector, arXiv:1407.4314.
- [64] J. Aguilar-Saavedra, A Minimal set of top anomalous couplings, Nucl.Phys. B812 (2009) 181–204, arXiv:0811.3842, doi:10.1016/j.nuclphysb.2008.12.012.
- [65] C. Zhang, S. Willenbrock, Effective-Field-Theory Approach to Top-Quark Production and Decay, Phys.Rev. D83 (2011) 034006, arXiv:1008.3869, doi:10.1103/PhysRevD.83.034006.
- [66] B. Grzadkowski, M. Iskrzynski, M. Misiak, J. Rosiek, Dimension-Six Terms in the Standard Model Lagrangian, JHEP 1010 (2010) 085, arXiv:1008.4884, doi:10.1007/JHEP10(2010)085.
- [67] Z. Hioki, K. Ohkuma, Latest constraint on nonstandard top-gluon couplings at hadron colliders and its future prospect, Phys.Rev. D88 (1) (2013) 017503, arXiv:1306.5387, doi:10.1103/PhysRevD.88.017503.
- [68] W. Bernreuther, P. Overmann, CP asymmetries in top quark pair production and decay: Contributions from neutral Higgs boson and gluino exchange, Z.Phys. C61 (1994) 599–606, doi:10.1007/BF01552627.
- [69] S. D. Rindani, Effect of anomalous  $t b W$  vertex on decay lepton distributions in  $e^+ e^-$  to  $t$  anti- $t$  and CP violating asymmetries, Pramana 54 (2000) 791–812, arXiv:hep-ph/0002006, doi:10.1007/s12043-000-0176-0.
- [70] B. Grzadkowski, Z. Hioki, Decoupling of anomalous top decay vertices in angular distribution of secondary particles, Phys.Lett. B557 (2003) 55–59, arXiv:hep-ph/0208079, doi:10.1016/S0370-2693(03)00187-4.
- [71] CMS Collaboration, Limits on the top-quark chromomagnetic dipole moment from angular distributions in  $t\bar{t}$  events at 7 TeV with the CMS detector, CMS-PAS-TOP-14-004.
- [72] A. Denner, S. Dittmaier, Reduction of one loop tensor five point integrals, Nucl.Phys. B658 (2003) 175–202, arXiv:hep-ph/0212259, doi:10.1016/S0550-3213(03)00184-6.
- [73] W. Giele, E. N. Glover, A Calculational formalism for one loop integrals, JHEP 0404 (2004) 029, arXiv:hep-ph/0402152, doi:10.1088/1126-6708/2004/04/029.
- [74] G. Passarino, M. Veltman, One Loop Corrections for  $e^+ e^-$  Annihilation Into  $\mu^+ \mu^-$  in the Weinberg Model, Nucl.Phys. B160 (1979) 151, doi:10.1016/0550-3213(79)90234-7.
- [75] T. Stelzer, W. Long, Automatic generation of tree level helicity amplitudes, Comput.Phys.Commun. 81 (1994) 357–371, arXiv:hep-ph/9401258, doi:10.1016/0010-4655(94)90084-1.

- [76] S. Catani, M. Seymour, A General algorithm for calculating jet cross-sections in NLO QCD, Nucl.Phys. B485 (1997) 291–419, arXiv:hep-ph/9605323, doi:10.1016/S0550-3213(96)00589-5.
- [77] S. Catani, S. Dittmaier, M. H. Seymour, Z. Trocsanyi, The Dipole formalism for next-to-leading order QCD calculations with massive partons, Nucl.Phys. B627 (2002) 189–265, arXiv:hep-ph/0201036, doi:10.1016/S0550-3213(02)00098-6.
- [78] K. Melnikov, M. Schulze, NLO QCD corrections to top quark pair production in association with one hard jet at hadron colliders, Nucl.Phys. B840 (2010) 129–159, arXiv:1004.3284, doi:10.1016/j.nuclphysb.2010.07.003.
- [79] K. Melnikov, A. Scharf, M. Schulze, Top quark pair production in association with a jet: QCD corrections and jet radiation in top quark decays, Phys.Rev. D85 (2012) 054002, arXiv:1111.4991, doi:10.1103/PhysRevD.85.054002.
- [80] A. Kardos, C. Papadopoulos, Z. Trocsanyi, Top quark pair production in association with a jet with NLO parton showering, Phys.Lett. B705 (2011) 76–81, arXiv:1101.2672, doi:10.1016/j.physletb.2011.09.080.
- [81] S. Alioli, S.-O. Moch, P. Uwer, Hadronic top-quark pair-production with one jet and parton showering, JHEP 1201 (2012) 137, arXiv:1110.5251, doi:10.1007/JHEP01(2012)137.
- [82] S. Alioli, P. Fernandez, J. Fuster, A. Irlles, S.-O. Moch, et al., A new observable to measure the top-quark mass at hadron colliders, Eur.Phys.J. C73 (2013) 2438, arXiv:1303.6415, doi:10.1140/epjc/s10052-013-2438-2.
- [83] Determination of the top-quark pole mass using tt +1-je t events collected with the ATLAS experiment in 7 TeV pp collisions, Tech. Rep. ATLAS-CONF-2014-053, CERN, Geneva (Sep 2014).
- [84] M. C. Smith, S. Willenbrock, QCD and Yukawa corrections to single top quark production via  $q\bar{q} \rightarrow t\bar{b}$ , Phys.Rev. D54 (1996) 6696–6702, arXiv:hep-ph/9604223, doi:10.1103/PhysRevD.54.6696.
- [85] T. Stelzer, Z. Sullivan, S. Willenbrock, Single Top Quark Production at Hadron Colliders, Phys. Rev. D58 (1998) 094021, arXiv:hep-ph/9807340, doi:10.1103/PhysRevD.58.094021.
- [86] Z. Sullivan, Understanding Single-Top-Quark Production and Jets at Hadron Colliders, Phys. Rev. D70 (2004) 114012, arXiv:hep-ph/0408049, doi:10.1103/PhysRevD.70.114012.
- [87] Z. Sullivan, Angular Correlations in Single-Top-Quark and Wjj Production at Next-To-Leading Order, Phys.Rev. D72 (2005) 094034, arXiv:hep-ph/0510224, doi:10.1103/PhysRevD.72.094034.
- [88] W. Giele, S. Keller, E. Laenen, QCD Corrections to W Boson Plus Heavy Quark Production at the Tevatron, Phys. Lett. B372 (1996) 141–149, arXiv:hep-ph/9511449, doi:10.1016/0370-2693(96)00078-0.
- [89] S. Zhu, Next-To-Leading Order QCD Corrections to  $bg \rightarrow tW^-$  at the CERN Large Hadron Collider, Phys. Lett. B524 (2002) 283–288, doi:10.1016/S0370-2693(01)01404-6.
- [90] P. Kant, O. Kind, T. Kintscher, T. Lohse, T. Martini, et al., HATHOR for single top-quark production: Updated predictions and uncertainty estimates for single top-quark production in hadronic collisions, arXiv:1406.4403.
- [91] M. Brucherseifer, F. Caola, K. Melnikov, On the NNLO QCD corrections to single-top production at the LHC, arXiv:1404.7116.
- [92] M. Assadsolimani, P. Kant, B. Tausk, P. Uwer, QCD two-loop corrections for hadronic single top-quark production in the t-channel, arXiv:1409.3654.
- [93] O. Tarasov, Connection between Feynman integrals having different values of the space-time dimension, Phys.Rev. D54 (1996) 6479–6490, arXiv:hep-th/9606018, doi:10.1103/PhysRevD.54.6479.
- [94] O. Tarasov, Generalized recurrence relations for two loop propagator integrals with arbitrary masses, Nucl.Phys. B502 (1997) 455–482, arXiv:hep-ph/9703319, doi:10.1016/S0550-3213(97)00376-3.
- [95] F. Tkachov, A Theorem on Analytical Calculability of Four Loop Renormalization Group Functions, Phys.Lett. B100 (1981) 65–68, doi:10.1016/0370-2693(81)90288-4.
- [96] K. Chetyrkin, F. Tkachov, Integration by Parts: The Algorithm to Calculate beta Functions in 4 Loops, Nucl.Phys. B192 (1981) 159–204, doi:10.1016/0550-3213(81)90199-1.
- [97] S. Laporta, High precision calculation of multiloop Feynman integrals by difference equations, Int.J.Mod.Phys. A15 (2000) 5087–5159, arXiv:hep-ph/0102033, doi:10.1016/S0217-751X(00)00215-7.
- [98] C. Studerus, Reduze-Feynman Integral Reduction in C++, Comput.Phys.Commun. 181 (2010) 1293–1300, arXiv:0912.2546, doi:10.1016/j.cpc.2010.03.012.
- [99] A. von Manteuffel, C. Studerus, Reduze 2 - Distributed Feynman Integral Reduction, arXiv:1201.4330.
- [100] P. Marquard, D. Seidel, unpublished.
- [101] G. Bell, Higher order QCD corrections in exclusive charmless B decays, arXiv:0705.3133.
- [102] G. Bell, NNLO vertex corrections in charmless hadronic B decays: Imaginary part, Nucl.Phys. B795 (2008) 1–26, arXiv:0705.3127, doi:10.1016/j.nuclphysb.2007.09.006.
- [103] G. Bell, NNLO vertex corrections in charmless hadronic B decays: Real part, Nucl.Phys. B822 (2009) 172–200, arXiv:0902.1915, doi:10.1016/j.nuclphysb.2009.07.012.
- [104] R. Bonciani, A. Ferroglia, Two-Loop QCD Corrections to the Heavy-to-Light Quark Decay, JHEP 0811 (2008) 065, arXiv:0809.4687, doi:10.1088/1126-6708/2008/11/065.
- [105] M. Beneke, T. Huber, X.-Q. Li, Two-loop QCD correction to differential semi-leptonic  $b \rightarrow u$  decays in the shape-function region, Nucl.Phys. B811 (2009) 77–97, arXiv:0810.1230, doi:10.1016/j.nuclphysb.2008.11.019.
- [106] H. Asatrian, C. Greub, B. Pecjak, NNLO corrections to  $\bar{B} \rightarrow X_u \ell \bar{\nu}$  in the shape-function region, Phys.Rev. D78 (2008) 114028, arXiv:0810.0987, doi:10.1103/PhysRevD.78.114028.
- [107] T. Huber, On a two-loop crossed six-line master integral with two massive lines, JHEP 0903 (2009) 024, arXiv:0901.2133, doi:10.1088/1126-6708/2009/03/024.
- [108] P. Kant, Finding Linear Dependencies in Integration-By-Parts Equations: A Monte Carlo Approach, Comput.Phys.Commun. 185 (2014) 1473–1476, arXiv:1309.7287, doi:10.1016/j.cpc.2014.01.017.
- [109] A. Czarnecki, M. Jezabek, J. H. Kuhn, Lepton Spectra From Decays of Polarized Top Quarks, Nucl.Phys. B351 (1991) 70–80, doi:10.1016/0550-3213(91)90082-9.
- [110] J. Gao, C. S. Li, H. X. Zhu, Top Quark Decay at Next-to-Next-to Leading Order in QCD, Phys.Rev.Lett. 110 (2013) 042001, arXiv:1210.2808, doi:10.1103/PhysRevLett.110.042001.
- [111] M. Brucherseifer, F. Caola, K. Melnikov,  $\mathcal{O}(\alpha_s^2)$  corrections to fully-differential top quark decays, JHEP 1304 (2013) 059, arXiv:1301.7133, doi:10.1007/JHEP04(2013)059.
- [112] W. Bernreuther, P. Gonzalez, C. Mellein, Decays of polarized top quarks to lepton, neutrino and jets at NLO QCD, Eur.Phys.J. C74 (2014) 2815, arXiv:1401.5930, doi:10.1140/epjc/s10052-014-2815-5.
- [113] S. Catani, Y. L. Dokshitzer, M. Olsson, G. Turnock, B. Weber, New clustering algorithm for multi-jet cross-sections in  $e^+e^-$  annihilation, Phys.Lett. B269 (1991) 432–438, doi:10.1016/0370-2693(91)90196-W.
- [114] W. Bernreuther, P. Gonzalez, M. Wiebusch, The Top Quark Decay Vertex in Standard Model Extensions, Eur.Phys.J. C60

- (2009) 197–211, arXiv:0812.1643, doi:10.1140/epjc/s10052-009-0887-4.
- [115] A. Czarnecki, J. G. Körner, J. H. Piclum, Helicity fractions of W bosons from top quark decays at NNLO in QCD, *Phys.Rev. D* 81 (2010) 111503, arXiv:1005.2625, doi:10.1103/PhysRevD.81.111503.
- [116] E. Shabalina, W helicity, top quark spin and charge, *EPJ Web Conf.* 49 (2013) 07002, doi:10.1051/epjconf/20134907002.
- [117] M. Juengst, Spin Correlation and W Helicity in Top Events with ATLAS, *PoS ICHEP2012* (2013) 220.
- [118] V. Khachatryan, et al., Measurement of the W boson helicity in events with a single reconstructed top quark in pp collisions at  $\sqrt{s} = 8$  TeV, arXiv:1410.1154.
- [119] B. Grzadkowski, M. Misiak, Anomalous Wtb coupling effects in the weak radiative B-meson decay, *Phys.Rev. D* 78 (2008) 077501, arXiv:0802.1413, doi:10.1103/PhysRevD.84.059903, 10.1103/PhysRevD.78.077501.
- [120] W. Bernreuther, M. Fuecker, Y. Umeda, Semileptonic decays of polarized top quarks: V + A admixture and QCD corrections, *Phys.Lett. B* 582 (2004) 32–38, arXiv:hep-ph/0308296, doi:10.1016/j.physletb.2003.12.010.
- [121] T. Binoth, G. Heinrich, An automatized algorithm to compute infrared divergent multiloop integrals, *Nucl.Phys. B* 585 (2000) 741–759, arXiv:hep-ph/0004013, doi:10.1016/S0550-3213(00)00429-6.
- [122] C. Anastasiou, K. Melnikov, F. Petriello, A new method for real radiation at NNLO, *Phys.Rev. D* 69 (2004) 076010, arXiv:hep-ph/0311311, doi:10.1103/PhysRevD.69.076010.
- [123] S. Weinzierl, Subtraction terms at NNLO, *JHEP* 0303 (2003) 062, arXiv:hep-ph/0302180, doi:10.1088/1126-6708/2003/03/062.
- [124] S. Frixione, M. Grazzini, Subtraction at NNLO, *JHEP* 0506 (2005) 010, arXiv:hep-ph/0411399, doi:10.1088/1126-6708/2005/06/010.
- [125] S. Catani, M. Grazzini, An NNLO subtraction formalism in hadron collisions and its application to Higgs boson production at the LHC, *Phys.Rev.Lett.* 98 (2007) 222002, arXiv:hep-ph/0703012, doi:10.1103/PhysRevLett.98.222002.
- [126] M. Czakon, A novel subtraction scheme for double-real radiation at NNLO, *Phys.Lett. B* 693 (2010) 259–268, arXiv:1005.0274, doi:10.1016/j.physletb.2010.08.036.
- [127] M. Czakon, Double-real radiation in hadronic top quark pair production as a proof of a certain concept, *Nucl.Phys. B* 849 (2011) 250–295, arXiv:1101.0642, doi:10.1016/j.nuclphysb.2011.03.020.
- [128] M. Czakon, D. Heymes, Four-dimensional formulation of the sector-improved residue subtraction scheme, arXiv:1408.2500.
- [129] D. A. Kosower, Antenna factorization of gauge theory amplitudes, *Phys.Rev. D* 57 (1998) 5410–5416, arXiv:hep-ph/9710213, doi:10.1103/PhysRevD.57.5410.
- [130] D. A. Kosower, Antenna factorization in strongly ordered limits, *Phys.Rev. D* 71 (2005) 045016, arXiv:hep-ph/0311272, doi:10.1103/PhysRevD.71.045016.
- [131] A. Gehrmann-De Ridder, T. Gehrmann, E. N. Glover, Antenna subtraction at NNLO, *JHEP* 0509 (2005) 056, arXiv:hep-ph/0505111, doi:10.1088/1126-6708/2005/09/056.
- [132] J. Currie, E. Glover, S. Wells, Infrared Structure at NNLO Using Antenna Subtraction, *JHEP* 1304 (2013) 066, arXiv:1301.4693, doi:10.1007/JHEP04(2013)066.
- [133] W. Bernreuther, C. Bogner, O. Dekkers, The real radiation antenna function for  $S \rightarrow Q\bar{Q}q\bar{q}$  at NNLO QCD, *JHEP* 1106 (2011) 032, arXiv:1105.0530, doi:10.1007/JHEP06(2011)032.
- [134] W. Bernreuther, C. Bogner, O. Dekkers, The real radiation antenna functions for  $S \rightarrow Q\bar{Q}gg$  at NNLO QCD, *JHEP* 1310 (2013) 161, arXiv:1309.6887, doi:10.1007/JHEP10(2013)161.
- [135] O. Dekkers, W. Bernreuther, The real-virtual antenna functions for  $S \rightarrow Q\bar{Q}X$  at NNLO QCD, *Phys.Lett. B* 738 (2014) 325–333, arXiv:1409.3124, doi:10.1016/j.physletb.2014.09.060.
- [136] A. Gehrmann-De Ridder, M. Ritzmann, NLO Antenna Subtraction with Massive Fermions, *JHEP* 0907 (2009) 041, arXiv:0904.3297, doi:10.1088/1126-6708/2009/07/041.
- [137] G. Abelof, A. Gehrmann-De Ridder, Antenna subtraction for the production of heavy particles at hadron colliders, *JHEP* 1104 (2011) 063, arXiv:1102.2443, doi:10.1007/JHEP04(2011)063.
- [138] G. Abelof, A. Gehrmann-De Ridder, Double real radiation corrections to  $t\bar{t}$  production at the LHC: the all-fermion processes, *JHEP* 1204 (2012) 076, arXiv:1112.4736, doi:10.1007/JHEP04(2012)076.
- [139] G. Abelof, O. Dekkers, A. Gehrmann-De Ridder, Antenna subtraction with massive fermions at NNLO: Double real initial-final configurations, *JHEP* 1212 (2012) 107, arXiv:1210.5059, doi:10.1007/JHEP12(2012)107.
- [140] G. Abelof, A. Gehrmann-De Ridder, P. Maierhofer, S. Pozzorini, NNLO QCD subtraction for top-antitop production in the  $q\bar{q}$  channel, *JHEP* 1408 (2014) 035, arXiv:1404.6493, doi:10.1007/JHEP08(2014)035.
- [141] G. Abelof, A. Gehrmann-De Ridder, Light fermionic NNLO QCD corrections to top-antitop production in the quark-antiquark channel, arXiv:1409.3148.
- [142] A. von Manteuffel, R. M. Schabinger, H. X. Zhu, The two-loop soft function for heavy quark pair production at future linear colliders, arXiv:1408.5134.
- [143] J. Gao, H. X. Zhu, Electroweak production of top-quark pairs in  $e^+e^-$  annihilation at NNLO in QCD: the vector contributions, arXiv:1408.5150.
- [144] C. Anastasiou, K. Melnikov, Higgs boson production at hadron colliders in NNLO QCD, *Nucl.Phys. B* 646 (2002) 220–256, arXiv:hep-ph/0207004, doi:10.1016/S0550-3213(02)00837-4.
- [145] A. Smirnov, Algorithm FIRE – Feynman Integral REduction, *JHEP* 0810 (2008) 107, arXiv:0807.3243, doi:10.1088/1126-6708/2008/10/107.
- [146] C. Anastasiou, A. Lazopoulos, Automatic integral reduction for higher order perturbative calculations, *JHEP* 0407 (2004) 046, arXiv:hep-ph/0404258, doi:10.1088/1126-6708/2004/07/046.
- [147] A. Kotikov, Differential equations method: New technique for massive Feynman diagrams calculation, *Phys.Lett. B* 254 (1991) 158–164, doi:10.1016/0370-2693(91)90413-K.
- [148] T. Gehrmann, E. Remiddi, Differential equations for two loop four point functions, *Nucl.Phys. B* 580 (2000) 485–518, arXiv:hep-ph/9912329, doi:10.1016/S0550-3213(00)00223-6.
- [149] E. Remiddi, J. Vermaseren, Harmonic polylogarithms, *Int.J.Mod.Phys. A* 15 (2000) 725–754, arXiv:hep-ph/9905237, doi:10.1142/S0217751X00000367.
- [150] J. Blümlein, Structural Relations of Harmonic Sums and Mellin Transforms up to Weight  $w = 5$ , *Comput.Phys.Commun.* 180 (2009) 2218–2249, arXiv:0901.3106, doi:10.1016/j.cpc.2009.07.004.
- [151] J. Ablinger, A Computer Algebra Toolbox for Harmonic Sums Related to Particle Physics, arXiv:1011.1176.
- [152] J. Ablinger, Computer Algebra Algorithms for Special Functions in Particle Physics, arXiv:1305.0687.
- [153] J. Ablinger, J. Blümlein, C. Schneider, Harmonic Sums and Polylogarithms Generated by Cyclotomic Polynomials, *J.Math.Phys.* 52 (2011) 102301, arXiv:1105.6063, doi:10.1063/1.3629472.
- [154] J. Ablinger, J. Blümlein, C. Schneider, Analytic and Algorithmic Aspects of Generalized Harmonic Sums and Polylogarithms, *J.Math.Phys.* 54 (2013) 082301, arXiv:1302.0378,

- doi:10.1063/1.4811117.
- [155] A. G. Kallen, A. Sabry, Fourth order vacuum polarization, *Kong.Dan.Vid.Sel.Mat.Fys.Med.* 29 (17) (1955) 1–20,
- [156] W. Bernreuther, R. Bonciani, T. Gehrmann, R. Heinesch, T. Leineweber, P. Mastrolia, E. Remiddi, Two-loop QCD corrections to the heavy quark form-factors: The Vector contributions, *Nucl.Phys. B706* (2005) 245–324, arXiv:hep-ph/0406046, doi:10.1016/j.nuclphysb.2004.10.059.
- [157] A. Hoang, J. H. Kühn, T. Teubner, Radiation of light fermions in heavy fermion production, *Nucl.Phys. B452* (1995) 173–187, arXiv:hep-ph/9505262, doi:10.1016/0550-3213(95)00308-F.
- [158] A. Czarnecki, K. Melnikov, Two loop QCD corrections to the heavy quark pair production cross-section in  $e^+e^-$  annihilation near the threshold, *Phys.Rev.Lett.* 80 (1998) 2531–2534, arXiv:hep-ph/9712222, doi:10.1103/PhysRevLett.80.2531.
- [159] M. Beneke, A. Signer, V. A. Smirnov, Two loop correction to the leptonic decay of quarkonium, *Phys.Rev.Lett.* 80 (1998) 2535–2538, arXiv:hep-ph/9712302, doi:10.1103/PhysRevLett.80.2535.
- [160] K. Chetyrkin, R. Harlander, J. H. Kühn, M. Steinhauser, Mass corrections to the vector current correlator, *Nucl.Phys. B503* (1997) 339–353, arXiv:hep-ph/9704222, doi:10.1016/S0550-3213(97)00383-0.
- [161] K. Chetyrkin, J. H. Kühn, M. Steinhauser, Three loop polarization function and  $O(\alpha_s^2)$  corrections to the production of heavy quarks, *Nucl.Phys. B482* (1996) 213–240, arXiv:hep-ph/9606230, doi:10.1016/S0550-3213(96)00534-2.
- [162] O. Dekkers, J. Ablinger, W. Bernreuther, J. Blümlein, to be published.
- [163] W. Bernreuther, R. Bonciani, T. Gehrmann, R. Heinesch, T. Leineweber, P. Mastrolia, E. Remiddi, Two-loop QCD corrections to the heavy quark form-factors: Axial vector contributions, *Nucl.Phys. B712* (2005) 229–286, arXiv:hep-ph/0412259, doi:10.1016/j.nuclphysb.2005.01.035.
- [164] W. Bernreuther, R. Bonciani, T. Gehrmann, R. Heinesch, T. Leineweber, E. Remiddi, Two-loop QCD corrections to the heavy quark form-factors: Anomaly contributions, *Nucl.Phys. B723* (2005) 91–116, arXiv:hep-ph/0504190, doi:10.1016/j.nuclphysb.2005.06.025.
- [165] W. Bernreuther, R. Bonciani, T. Gehrmann, R. Heinesch, P. Mastrolia, E. Remiddi, Decays of scalar and pseudoscalar Higgs bosons into fermions: Two-loop QCD corrections to the Higgs-quark-antiquark amplitude, *Phys.Rev. D72* (2005) 096002, arXiv:hep-ph/0508254, doi:10.1103/PhysRevD.72.096002.
- [166] W. Bernreuther, R. Bonciani, T. Gehrmann, R. Heinesch, T. Leineweber, P. Mastrolia, E. Remiddi, QCD corrections to static heavy quark form-factors, *Phys.Rev.Lett.* 95 (2005) 261802, arXiv:hep-ph/0509341, doi:10.1103/PhysRevLett.95.261802.
- [167] W. Bernreuther, R. Bonciani, T. Gehrmann, R. Heinesch, T. Leineweber, P. Mastrolia, E. Remiddi, Heavy-quark form-factors and threshold cross section at  $O(\alpha_s^2)$ , *PoS HEP2005* (2006) 229, arXiv:hep-ph/0601207.
- [168] S. Catani, M. H. Seymour, Corrections of  $O(\alpha_s^2)$  to the forward backward asymmetry, *JHEP* 9907 (1999) 023, arXiv:hep-ph/9905424, doi:10.1088/1126-6708/1999/07/023.
- [169] W. Bernreuther, R. Bonciani, T. Gehrmann, R. Heinesch, T. Leineweber, P. Mastrolia, E. Remiddi, Two-Parton Contribution to the Heavy-Quark Forward-Backward Asymmetry in NNLO QCD, *Nucl.Phys. B750* (2006) 83–107, arXiv:hep-ph/0604031, doi:10.1016/j.nuclphysb.2006.05.031.
- [170] K. Waniger, Die Vorwärts-Rückwärts-Asymmetrie für schwere Quarks zur Ordnung  $\alpha_s^2$ , Doctoral Thesis RWTH Aachen (2011).
- [171] K. Hasegawa, S. Moch, P. Uwer, AutoDipole: Automated generation of dipole subtraction terms, *Comput.Phys.Commun.* 181 (2010) 1802–1817, arXiv:0911.4371, doi:10.1016/j.cpc.2010.06.044.
- [172] K. Hasegawa, Super AutoDipole, *Eur.Phys.J. C70* (2010) 285–293, arXiv:1007.1585, doi:10.1140/epjc/s10052-010-1452-x.
- [173] R. Lewis, Fermat—A computer algebra system for polynomial and matrix computation.
- [174] D. J. Broadhurst, Three loop on-shell charge renormalization without integration: Lambda-MS (QED) to four loops, *Z.Phys. C54* (1992) 599–606, doi:10.1007/BF01559486.
- [175] L. V. Avdeev, Recurrence relations for three loop prototypes of bubble diagrams with a mass, *Comput.Phys.Commun.* 98 (1996) 15–19, arXiv:hep-ph/9512442, doi:10.1016/0010-4655(96)00090-2.
- [176] M. Steinhauser, MATAD: A Program package for the computation of MAssive TADpoles, *Comput.Phys.Commun.* 134 (2001) 335–364, arXiv:hep-ph/0009029, doi:10.1016/S0010-4655(00)00204-6.
- [177] Y. Schröder, A. Vuorinen, High-precision epsilon expansions of single-mass-scale four-loop vacuum bubbles, *JHEP* 0506 (2005) 051, arXiv:hep-ph/0503209, doi:10.1088/1126-6708/2005/06/051.
- [178] J. Usovitsch, Reduktion von Mehrschleifen-Skalar-Integralen auf Master-Integrale mit dem Laporta-Algorithmus, Master Thesis, Humboldt-Universität zu Berlin (2014).